

Extended Skyrme interactions for nuclear matter, finite nuclei and neutron stars

Zhen Zhang¹ and Lie-Wen Chen^{*1,2}

¹*Department of Physics and Astronomy and Shanghai Key Laboratory for Particle Physics and Cosmology, Shanghai Jiao Tong University, Shanghai 200240, China*

²*Center of Theoretical Nuclear Physics, National Laboratory of Heavy Ion Accelerator, Lanzhou 730000, China*

(Dated: September 3, 2018)

Recent progress in theory, experiment and observation challenges the mean field models using the conventional Skyrme interaction, suggesting that the extension of the conventional Skyrme interaction is necessary. In this work, by fitting the experimental data of a number of finite nuclei together with a few additional constraints on nuclear matter using the simulated annealing method, we construct three Skyrme interaction parameter sets, namely, eMSL07, eMSL08 and eMSL09, based on an extended Skyrme interaction which includes additional momentum and density dependent two-body forces to effectively simulate the momentum dependence of the three-body force. The three new interactions can reasonably describe the ground-state properties and the isoscalar giant monopole resonance energies of various spherical nuclei used in the fit as well as the ground-state properties of many other spherical nuclei, nicely conform to the current knowledge on the equation of state of asymmetric nuclear matter, eliminate the notorious unphysical instabilities of symmetric nuclear matter and pure neutron matter up to a very high density of 1.2 fm^{-3} , and simultaneously support heavier neutron stars with mass larger than two times solar mass. One important difference of the three new interactions is about the prediction of the symmetry energy at supra-saturation densities, and these new interactions are thus potentially useful for the determination of the largely uncertain high-density symmetry energy in future. In addition, a comparison is made for the predictions of nuclear matter, finite nuclei and neutron stars with the three new interactions versus those with three typical interactions BSk22, BSk24 and BSk26 from Brussels group.

PACS numbers: 21.65.Ef, 21.30.Fe, 21.60.Jz, 26.60.Dd

I. INTRODUCTION

The exact knowledge on infinite nuclear matter, which is intimately related to the in-medium effective nuclear interactions, is of fundamental importance in nuclear physics and astrophysics [1–4]. Especially, the equation of state (EOS) of isospin asymmetric nuclear matter is the main ingredient in the study of neutron stars. In principle, the nuclear matter EOS can be obtained from various microscopic many-body approaches, e.g., the nonrelativistic and relativistic Brueckner-Hartree-Fock (BHF) method [5–7], the variational many-body approach [8, 9], quantum Monte Carlo (QMC) method [10–12] and chiral effective field theory (ChEFT) [13, 14], using realistic nuclear forces. However, due to the poorly known many-body interactions and the limitations in the techniques for solving the nuclear many-body problem, accurate determination of properties of nuclear matter around and beyond saturation density ρ_0 is still an open challenge for microscopic many-body theory. Another different perspective is the mean field model using phenomenological nuclear effective interactions with several parameters adjusted by fitting experimental data [15]. Among various phenomenological interactions, the nonrelativistic zero-range density and momentum-dependent Skyrme-type effective nucleon-nucleon interactions perhaps are the most

widely used. Proposed by Skyrme in the 1950s [16] and firstly applied in the study of finite nuclei in Hartree-Fock (HF) calculations by Brink and Vautherin in 1970s [17], the Skyrme interaction enormously simplifies the calculations with its zero-range form and has been very successfully used to describe the masses, charge radii and excited states of finite nuclei as well as the EOS of nuclear matter around ρ_0 . Moreover, extrapolation to high-density region based on the Skyrme-Hartree-Fock (SHF) model provides an important approach to investigate the properties of dense nuclear matter and the relevant astrophysics problems, especially the properties of neutron stars.

Since 1970s, a lot of work has been devoted to improving the Skyrme interaction to better reproduce the experimental data or describe different physical objects. Recently, much attention has been given to the problem of searching for effective interactions or energy density functionals (EDFs) which could simultaneously reproduce the properties of nuclear matter and finite nuclei, and at the same time be applicable for the study of neutron stars [15, 18–30]. This problem is of particular interest as two very heavy neutron stars with mass of two times solar mass ($2M_\odot$) have been observed recently [31, 32], which requires the pressure of high-density nuclear matter should be large enough to support such massive neutron stars against the strong gravity. This requirement is a big challenge for many theoretical models and indeed rules out essentially all the soft nuclear matter EOSs. Given the EOS of symmetric nuclear matter has been relatively well constrained even up to about $5\rho_0$

*Corresponding author (email: lwchen@sjtu.edu.cn)

by analyzing the experimental data on giant resonances of finite nuclei [33–35] as well as the collective flows and kaon production in heavy-ion collisions [36–38], a softer symmetry energy at high densities has been essentially ruled out by the observation of $2M_{\odot}$ neutron stars. It should be pointed out that some new physical mechanisms, such as non-Newtonian gravity [39–42], may support $2M_{\odot}$ neutron stars with a soft symmetry energy. In the present work we shall focus on the standard nuclear physics without considering these new physics.

During the last decade, considerable progress in determining the symmetry energy or neutron matter EOS at subsaturation densities has been made, both theoretically and experimentally. Indeed, it has been well established that the binding energy of finite nuclei can put rather stringent constraints on the symmetry energy at a subsaturation density $\rho \approx (2/3)\rho_0$ [43–48]. For the symmetry energy at an even lower density $\rho \approx \rho_0/3$, it has been shown recently [49] that the measurement of the electric dipole polarizability in ^{208}Pb can give a quite accurate constraint and the result is in very good agreement with the constraints from SHF analyses of isobaric analog states and neutron skin data [46] as well as the transport model analyses of mid-peripheral heavy-ion collisions of Sn isotopes [50]. For pure neutron matter, very similarly, the binding energy per neutron around subsaturation densities $(2/3)\rho_0$ and $\rho_0/3$ has been constrained recently by analyzing the ground-state properties of doubly magic nuclei [48] and the electric dipole polarizability in ^{208}Pb [49], respectively. In addition, the calculations based on the microscopic ChEFT [14] as well as the QMC calculations [10–12] have also provided very useful information on the EOS of pure neutron matter, especially at subsaturation densities. These theoretical and experimental constraints consistently favor a relatively soft symmetry energy or EOS of asymmetric nuclear matter, at least at subsaturation densities around $(2/3)\rho_0$. The symmetry energy softer at subsaturation densities (favored by experimental constraints and theoretical predictions) but stiffer at higher densities (favored by the observation of $2M_{\odot}$ neutron stars) challenges the SHF model with the conventional Skyrme interactions. For example, the Skyrme interaction TOVmin [26], which is built by fitting properties of both finite nuclei and neutron stars, can successfully support $2M_{\odot}$ neutron stars but predicts a neutron matter EOS significantly deviating from the ChEFT calculations [14] as well as the constraint extracted from analyzing the electric dipole polarizability in ^{208}Pb [49] at densities below about $0.5\rho_0$.

Furthermore, it is well known that a notorious shortcoming of the conventional standard Skyrme interactions is that they predict various instabilities of nuclear matter around saturation density or at supra-saturation densities, which in principle hinders the application of the Skyrme interactions in the study of dense nuclear matter as well as neutron stars. For instance, most of the conventional standard Skyrme interactions predict spin or

spin-isospin polarization in the density region of about $(1 \sim 3.5)\rho_0$ [24, 52], including the famous SLy4 interaction [19] which has been widely used in both nuclear physics and neutron star studies and leads to spin-isospin instability of symmetric nuclear matter at densities beyond about $2\rho_0$ [51]. On the other hand, the calculations based on the microscopic many-body theory using realistic nuclear forces, such as relativistic and nonrelativistic BHF approach [53, 54], the QMC method [55], the ChEFT method [56], and the lowest order constrained variational approach [57], predict no such instabilities at densities up to substantially high densities. To solve this problem, Margueron and Sagawa proposed an extended form of the Skyrme interaction with additional density-dependent terms [58], while Chamel *et al.* introduced momentum and density dependent terms which are density-dependent generalizations of the usual t_1 and t_2 terms in the conventional standard Skyrme interaction [22]. In Ref. [51], Chamel and Goriely find that the spin and spin-isospin instabilities can be removed by omitting the time-odd terms in $(\mathbf{s}_n + \mathbf{s}_p) \times (\mathbf{T}_n + \mathbf{T}_p)$ and $(\mathbf{s}_n - \mathbf{s}_p) \times (\mathbf{T}_n - \mathbf{T}_p)$, namely setting $C_0^T = C_1^T = 0$ in the notation of Ref. [59].

In Ref. [24], Dutra *et al.* find that, of 240 standard Skyrme interactions, only 6 satisfy all eleven constraints on the properties of nuclear matter selected therein. However, we would like to point out that all the 6 Skyrme interactions predict spin or spin-isospin instabilities below $3\rho_0$ and fail to produce $2M_{\odot}$ neutron stars. In addition, the Skyrme interactions constrained only from nuclear matter properties usually have no common ability to reproduce properties of finite nuclei [60]. A feasible approach to address the above problems existed in the conventional standard Skyrme interactions is to extend the Skyrme interaction by including additional terms to effectively simulate the momentum dependence of the three-body force [22, 23, 27, 30, 61–63]. In this work, based on the extended Skyrme interaction, we use the simulated annealing method [64] to construct three Skyrme interaction parameter sets, namely, eMSL07, eMSL08 and eMSL09, by fitting the experimental data of ground-state properties and isoscalar giant monopole resonance (ISGMR) energies of some finite nuclei together with a few additional constraints on properties of nuclear matter. Our main purpose here is to construct parameter sets of the extended Skyrme interaction that can reasonably describe the properties of finite (closed-shell or semi-closed-shell) nuclei, satisfy the most recent constraints on nuclear matter, especially the EOS of asymmetric nuclear matter at subsaturation densities, eliminate the unphysical instabilities of nuclear matter in the density region encountered in neutron stars, and successfully support $2M_{\odot}$ neutron stars. In addition, a comparison is made for the predictions of nuclear matter, finite nuclei and neutron stars with the new interactions constructed in the present work versus those with the accurately calibrated interactions BSk22, BSk24 and BSk26 [27] from Brussels group. Although constructed with a different strategy from that

of the Brussels group, the new extended Skyrme interactions obtained in the present work give predictions for nuclear matter and neutron stars that are very similar with the calculations using the extended Skyrme interactions in BSk family [27], which are constructed mainly for accurately describing the nuclear mass. Furthermore, although the three new interactions constructed in the present work give very similar predictions of the properties of finite nuclei as well as nuclear matter at subsaturation densities, they predict different supra-saturation density behaviors of the symmetry energy, and these new interactions are thus potentially useful for the determination of the largely uncertain high-density symmetry energy in future.

The paper is organized as follows. In Sec. II, we introduce the form of the extended Skyrme interaction and the energy density functional adopted in this work. In Sec. III, the experimental data and constraints used in our fitting are presented. The parameter sets of three new extended Skyrme interactions and the corresponding results are exhibited in Sec. IV. Finally, we summarize our conclusions in Sec. V. Appendix A gives the expressions for several macroscopic quantities in the extended SHF model and Appendix B presents the analytical relations between the chosen macroscopic quantities and the microscopic Skyrme parameters.

II. MODELS AND METHODS

A. Extended Skyrme-Hartree-Fock model

In the conventional SHF model, nucleons generally interact with each other through the so-called standard Skyrme interaction (see, e.g., Ref. [18])

$$\begin{aligned}
v(\mathbf{r}_1, \mathbf{r}_2) = & t_0(1 + x_0 P_\sigma) \delta(\mathbf{r}_1 - \mathbf{r}_2) \\
& + \frac{1}{2} t_1(1 + x_1 P_\sigma) [\mathbf{k}'^2 \delta(\mathbf{r}_1 - \mathbf{r}_2) + \text{c.c.}] \\
& + t_2(1 + x_2 P_\sigma) \mathbf{k}' \cdot \delta(\mathbf{r}_1 - \mathbf{r}_2) \mathbf{k} \\
& + \frac{1}{6} t_3(1 + x_3 P_\sigma) \rho^\alpha \left(\frac{\mathbf{r}_1 + \mathbf{r}_2}{2} \right) \delta(\mathbf{r}_1 - \mathbf{r}_2) \\
& + i W_0 (\boldsymbol{\sigma}_1 + \boldsymbol{\sigma}_2) \cdot [\mathbf{k}' \times \delta(\mathbf{r}_1 - \mathbf{r}_2) \mathbf{k}], \quad (1)
\end{aligned}$$

where $\boldsymbol{\sigma}_i$ is the Pauli spin operator, P_σ is the spin-exchange operator, $\mathbf{k} = -i(\nabla_1 - \nabla_2)/2$ is the relative momentum operator, and \mathbf{k}' is the conjugate operator of \mathbf{k} acting on the left.

In the present work, to effectively take account of the momentum dependence of the three body interaction, we use the extended Skyrme interaction with the following additional zero-range density- and momentum-dependent terms [22, 23, 27, 30, 61–63]

$$\begin{aligned}
& + \frac{1}{2} t_4(1 + x_4 P_\sigma) \left[\mathbf{k}'^2 \rho^\beta \left(\frac{\mathbf{r}_1 + \mathbf{r}_2}{2} \right) \delta(\mathbf{r}_1 - \mathbf{r}_2) + \text{c.c.} \right] \\
& + t_5(1 + x_5 P_\sigma) \mathbf{k}' \cdot \rho^\gamma \left(\frac{\mathbf{r}_1 + \mathbf{r}_2}{2} \right) \delta(\mathbf{r}_1 - \mathbf{r}_2) \mathbf{k}, \quad (2)
\end{aligned}$$

which are just the density dependent generalization of the t_1 and t_2 terms in Eq. (1). For simplicity, β and γ are set to be unity in the present work, just like the form used in Ref. [61–63]. It should be noted that in HF calculations the zero-range momentum dependent three-body force is equivalent to a momentum and density dependent two-body force for spin-saturated systems, and the original values of β and γ are just unity [65]. Therefore, there are thirteen adjustable Skyrme parameters $t_0 \sim t_5$, $x_0 \sim x_5$ and α in the present extended Skyrme interaction.

In Hartree-Fock approach with the extended Skyrme interaction, the total energy density of a nucleus can be expressed as

$$\mathcal{H} = \mathcal{K} + \mathcal{H}_0 + \mathcal{H}_3 + \mathcal{H}_{\text{eff}} + \mathcal{H}_{\text{fin}} + \mathcal{H}_{\text{SO}} + \mathcal{H}_{\text{sg}} + \mathcal{H}_{\text{Coul}}, \quad (3)$$

where $\mathcal{K} = \frac{\hbar^2}{2m} \tau$ is the kinetic-energy term and \mathcal{H}_0 , \mathcal{H}_3 , \mathcal{H}_{eff} , \mathcal{H}_{fin} , \mathcal{H}_{SO} , \mathcal{H}_{sg} are given by [22]

$$\mathcal{H}_0 = \frac{1}{4} t_0 [(2 + x_0) \rho^2 - (2x_0 + 1)(\rho_n^2 + \rho_p^2)], \quad (4)$$

$$\mathcal{H}_3 = \frac{1}{24} t_3 \rho^\alpha [(2 + x_3) \rho^2 - (2x_3 + 1)(\rho_n^2 + \rho_p^2)], \quad (5)$$

$$\begin{aligned}
\mathcal{H}_{\text{eff}} = & \frac{1}{8} [t_1(2 + x_1) + t_2(2 + x_2)] \rho \tau \\
& - \frac{1}{8} [t_1(2x_1 + 1) - t_2(2x_2 + 1)] (\rho_n \tau_n + \rho_p \tau_p), \\
& + \frac{1}{8} [t_4(2 + x_4) \rho^\beta + t_5(2 + x_5) \rho^\gamma] \rho \tau \\
& - \frac{1}{8} [t_4(2x_4 + 1) \rho^\beta - t_5(2x_5 + 1) \rho^\gamma] (\rho_n \tau_n + \rho_p \tau_p), \quad (6)
\end{aligned}$$

$$\begin{aligned}
\mathcal{H}_{\text{fin}} = & \frac{1}{32} [3t_1(2 + x_1) - t_2(2 + x_2)] (\nabla \rho)^2 \\
& - \frac{1}{32} [3t_1(2x_1 + 1) + t_2(2x_2 + 1)] \sum_{q=n,p} (\nabla \rho_q)^2 \\
& + \frac{1}{32} [(2\beta + 3)t_4(2 + x_4) \rho^\beta - t_5(2 + x_5) \rho^\gamma] (\nabla \rho)^2 \\
& - \frac{1}{32} [3t_4(2x_4 + 1) \rho^\beta + t_5(2x_5 + 1) \rho^\gamma] \sum_{q=n,p} (\nabla \rho_q)^2 \\
& - \frac{\beta}{16} t_4(2x_4 + 1) \rho^{\beta-1} \nabla \rho \sum_{q=n,p} \rho_q \nabla \rho_q, \quad (7)
\end{aligned}$$

$$\mathcal{H}_{\text{SO}} = \frac{1}{2} W_0 [J \cdot \nabla \rho + J_n \nabla \rho_n + J_p \nabla \rho], \quad (8)$$

$$\begin{aligned}
\mathcal{H}_{\text{sg}} = & -\frac{1}{16} (t_1 x_1 + t_2 x_2) J^2 + \frac{1}{16} (t_1 - t_2) \sum_{q=n,p} J_q^2 \\
& - \frac{1}{16} (t_4 x_4 \rho^\beta + t_5 x_5 \rho^\gamma) J^2 \\
& + \frac{1}{16} (t_4 \rho^\beta - t_5 \rho^\gamma) \sum_{q=n,p} J_q^2. \quad (9)
\end{aligned}$$

Here, $\rho = \rho_n + \rho_p$, $\tau = \tau_n + \tau_p$, and $J = J_p + J_n$ are the particle number density, kinetic-energy density, and

spin density, with p and n denoting the protons and neutrons, respectively. The Coulomb energy density can be expressed as

$$\mathcal{H}_{\text{Coul}} = \mathcal{H}_{\text{Coul}}^{\text{dir}} + \mathcal{H}_{\text{Coul}}^{\text{exc}}, \quad (10)$$

where $\mathcal{H}_{\text{Coul}}^{\text{dir}}$ is the direct term of the form

$$\mathcal{H}_{\text{Coul}}^{\text{dir}} = \frac{1}{2}e^2\rho_p(r) \int \frac{\rho_p(r')d^3r'}{|\mathbf{r} - \mathbf{r}'|}, \quad (11)$$

and $\mathcal{H}_{\text{Coul}}^{\text{exc}}$ is the exchange term

$$\mathcal{H}_{\text{Coul}}^{\text{exc}}(r) = -\frac{3}{4}e^2\rho_p(r) \left(\frac{3\rho_p(r)}{\pi} \right)^{1/3}. \quad (12)$$

In the present work, we include the center-of-mass correction in the first order to the binding energy by modifying nucleon mass m to $mA/(A-1)$ with A the nucleon number. The pairing energy is evaluated in the constant gap approximation with the gap [66]

$$\Delta = \frac{11.2}{\sqrt{A}} \text{MeV}. \quad (13)$$

We would also like to point out that the contributions of spin current tensor terms J^2 and J_q^2 are also included in our calculations.

B. Skyrme parameters and macroscopic quantities of nuclear matter

The expression Eq. (3) can be rewritten as

$$\begin{aligned} \mathcal{H} = & \mathcal{K} + \mathcal{H}_0 + \mathcal{H}_3 + \mathcal{H}_{\text{eff}} + \frac{G_S}{2}(\nabla\rho)^2 - \frac{G_V}{2}(\nabla\rho_1)^2 \\ & - \frac{G_{SV}}{2}\delta\nabla\rho\nabla\rho_1 + \mathcal{H}_{\text{Coul}} + \mathcal{H}_{\text{SO}} + \mathcal{H}_{\text{sg}}, \end{aligned} \quad (14)$$

where G_S is the gradient coefficient, G_V is the symmetry-gradient coefficient, G_{SV} is the cross gradient coefficient, and $\delta = \rho_1/\rho$ is the isospin asymmetry with $\rho_1 = \rho_n - \rho_p$. In the limit of infinite static nuclear matter, the sum of $\mathcal{K} + \mathcal{H}_0 + \mathcal{H}_3 + \mathcal{H}_{\text{eff}}$ corresponds to the nuclear matter energy density $\rho E(\rho, \delta)$ where $E(\rho, \delta)$ is just the EOS of asymmetric nuclear matter. Conventionally, some macroscopic quantities are introduced to characterize the EOS of asymmetric nuclear matter. For example, the $E(\rho, \delta)$ can be expanded as

$$E(\rho, \delta) = E_0(\rho) + E_{\text{sym}}(\rho)\delta^2 + \mathcal{O}(\delta^4), \quad (15)$$

where $E_0(\rho)$ is the EOS of symmetric nuclear matter and $E_{\text{sym}}(\rho)$ is the symmetry energy. The $E_0(\rho)$ is usually expanded around saturation density ρ_0 in terms of the incompressibility coefficient K_0 and the skewness coefficient J_0 as

$$E_0 = E_0(\rho_0) + \frac{1}{2!}K_0\chi^2 + \frac{1}{3!}J_0\chi^3 + \mathcal{O}(\chi^4), \quad (16)$$

with $\chi = (\rho - \rho_0)/(3\rho_0)$. Similarly, the $E_{\text{sym}}(\rho)$ can be expanded around a reference density ρ_r in terms of the density slope parameter L and the density curvature parameter K_{sym} as

$$\begin{aligned} E_{\text{sym}}(\rho) = & E_{\text{sym}}(\rho_r) + L(\rho_r)\chi_r \\ & + \frac{1}{2!}K_{\text{sym}}(\rho_r)\chi_r^2 + \mathcal{O}(\chi_r^3), \end{aligned} \quad (17)$$

with $\chi_r = (\rho - \rho_r)/(3\rho_r)$. The $E_0(\rho_0)$, K_0 , J_0 , $E_{\text{sym}}(\rho_r)$, $L(\rho_r)$ and $K_{\text{sym}}(\rho_r)$ are six important macroscopic quantities that characterize the EOS of asymmetric nuclear matter.

According to the analysis method in the modified Skyrme-like (MSL) model with the standard Skyrme interaction [67, 68], the nine Skyrme parameters $t_0 \sim t_3$, $x_0 \sim x_3$ and α are expressed explicitly in terms of nine macroscopic quantities ρ_0 , $E_0(\rho_0)$, K_0 , $E_{\text{sym}}(\rho_r)$, $L(\rho_r)$, G_S , G_V , the isoscalar effective mass at saturation density $m_{s,0}^*$ and isovector effective mass at saturation density $m_{v,0}^*$. For the extended Skyrme interaction with thirteen Skyrme parameters in the present work, four additional macroscopic quantities are needed to determine the thirteen Skyrme parameters, and here we use the skewness coefficient J_0 , the density curvature parameter of the symmetry energy $K_{\text{sym}}(\rho_r)$, the cross gradient coefficient G_{SV} and the Landau parameter $G'_0(\rho_0)$ of symmetric nuclear matter in the spin-isospin channel. Here J_0 and $K_{\text{sym}}(\rho_r)$, two higher-order quantities in nuclear matter EOS, may have important impacts on neutron star properties but are still poorly known [67, 69, 70]. The coefficient G_{SV} vanishes in the standard SHF model. The Landau parameter G'_0 determines, to the leading order, the spin-isospin properties of nuclear matter and its value at saturation density can vary from about 0 to 1.6 depending on the models and methods [59, 64, 71–76]. In Appendix A, we present the explicit expressions of several macroscopic quantities in the SHF model with the extended Skyrme interactions. And the analytical relations between the thirteen macroscopic quantities, i.e., ρ_0 , $E_0(\rho_0)$, K_0 , J_0 , $E_{\text{sym}}(\rho_r)$, $L(\rho_r)$, $K_{\text{sym}}(\rho_r)$, G_S , G_V , G_{SV} , $m_{s,0}^*$, $m_{v,0}^*$ and G'_0 , and the thirteen Skyrme parameters $t_0 \sim t_5$, $x_0 \sim x_5$ and α with fixed β and γ can be found in Appendix B.

The MSL method, in which all the Skyrme parameters are expressed in terms of macroscopic quantities, provides a simple and convenient approach to consider theoretical, experimental or empirical constraints on the selected macroscopic quantities for the properties of asymmetric nuclear matter in the SHF calculations. Another important advantage of the MSL method is that one can easily examine the correlation of experimental data or observations with each individual macroscopic quantities by varying individually these macroscopic quantities within their empirical ranges [68]. In the present work, instead of making correlation analysis, we shall focus on building parameter sets of the extended Skyrme interactions.

C. Landau parameters

The stability of nuclear matter can be investigated using the Landau Fermi-liquid theory. In this approach, for symmetric nuclear matter, the interaction $V(\mathbf{k}, \mathbf{k}')$ between two quasiparticles at Fermi surface with momentum \mathbf{k} and \mathbf{k}' is obtained from a second-order variation of the energy density \mathcal{E} with respect to a variation of distribution function of the quasiparticles, and it can be usually written as

$$V(\mathbf{k}, \mathbf{k}') = \delta(\mathbf{r})N_0^{-1} \sum_l [F_l + F'_l \boldsymbol{\tau}_i \cdot \boldsymbol{\tau}_j + G_l \boldsymbol{\sigma}_i \cdot \boldsymbol{\sigma}_j + G'_l (\boldsymbol{\tau}_i \cdot \boldsymbol{\tau}_j) (\boldsymbol{\sigma}_i \cdot \boldsymbol{\sigma}_j)] P_l(\cos\theta), \quad (18)$$

where P_l is the Legendre polynomial, θ is the angle between \mathbf{k} and \mathbf{k}' , and N_0 is the level density at the Fermi surface defined as

$$N_0 = \frac{2m_s^* k_F}{\hbar^2 \pi^2}, \quad (19)$$

where $k_F = (3\pi^2 \rho/2)^{1/3}$ is the Fermi momentum and m_s^* is the isoscalar effective mass at density ρ . F_l , F'_l , G_l and G'_l are the so-called dimensionless Landau parameters. For the Skyrme interaction containing only S and P wave contributions that we are considering in the present work, all Landau parameters vanish for $l > 1$. Therefore, there are eight Landau parameters for symmetric nuclear matter, i.e., F_l , F'_l , G_l and G'_l ($l = 0, 1$). Explicit expressions of the Landau parameters for the extended Skyrme energy functional can be found in Ref. [22].

The Landau stability conditions

$$F_l > -(2l + 1), \quad (20)$$

$$F'_l > -(2l + 1), \quad (21)$$

$$G_l > -(2l + 1), \quad (22)$$

$$G'_l > -(2l + 1), \quad (23)$$

guarantee the stability of symmetric nuclear matter against distortions of the momentum distribution functions in different channels. It is of particular interest to see that the conditions on F_0 , F'_0 , G_0 and G'_0 of symmetric nuclear matter ensure the stabilities of symmetric nuclear matter against spinodal instability, isospin instability, ferromagnetic instability and spin-isospin instability, respectively, which can be easily seen through the following relationships [23, 59]

$$\frac{\hbar^2 k_F^2}{3m_s^*} (1 + F_0) = \left. \frac{\partial^2 \mathcal{E}(\rho, \rho_1, s_0, s_1)}{\partial \rho^2} \right|_{\rho_1=s_0=s_1=0}, \quad (24)$$

$$\frac{\hbar^2 k_F^2}{3m_s^*} (1 + F'_0) = \left. \frac{\partial^2 \mathcal{E}(\rho, \rho_1, s_0, s_1)}{\partial (\rho_1)^2} \right|_{\rho_1=s_0=s_1=0}, \quad (25)$$

$$\frac{\hbar^2 k_F^2}{3m_s^*} (1 + G_0) = \left. \frac{\partial^2 \mathcal{E}(\rho, \rho_1, s_0, s_1)}{\partial (s_0)^2} \right|_{\rho_1=s_0=s_1=0}, \quad (26)$$

$$\frac{\hbar^2 k_F^2}{3m_s^*} (1 + G'_0) = \left. \frac{\partial^2 \mathcal{E}(\rho, \rho_1, s_0, s_1)}{\partial (s_1)^2} \right|_{\rho_1=s_0=s_1=0}, \quad (27)$$

where \mathcal{E} represents the energy density of nuclear matter. Here, in the notation of Ref. [59], $\rho_1 = (\rho_n - \rho_p)$ is the isovector scalar density, $s_0 = (\rho_{n\uparrow} - \rho_{n\downarrow} + \rho_{p\uparrow} - \rho_{p\downarrow})$ is the isoscalar vector density and $s_1 = (\rho_{n\uparrow} - \rho_{n\downarrow} - \rho_{p\uparrow} + \rho_{p\downarrow})$ the isovector vector density with \uparrow (\downarrow) denoting spin-up (-down). For usual nuclear matter with spin saturation, one has the EOS $E(\rho, \delta) = \mathcal{E}(\rho, \rho_1, 0, 0)/\rho$, the incompressibility $K(\rho) = 18\rho \frac{\partial E}{\partial \rho} + 9\rho^2 \frac{\partial^2 E}{\partial \rho^2}$ and $E_{\text{sym}}(\rho) = \frac{1}{2} \frac{\partial^2 E}{\partial \delta^2} |_{\delta=0}$, and then one can obtain from Eqs. (24) and (25) the following relations

$$K(\rho) = \frac{3\hbar^2 k_F^2}{m_s^*} (1 + F_0), \quad (28)$$

$$E_{\text{sym}}(\rho) = \frac{\hbar^2 k_F^2}{6m_s^*} (1 + F'_0). \quad (29)$$

In addition, F_1 and F'_1 are directly related to the isoscalar and isovector effective masses through the following expressions [23]

$$\frac{m_s^*}{m} = 1 + \frac{F_1}{3}, \quad (30)$$

$$\frac{m_s^*}{m_v^*} = 1 + \frac{F'_1}{3}. \quad (31)$$

The conditions $F_1 > -3$ and $F'_1 > -3$ are thus naturally satisfied at arbitrary densities for positive isoscalar and isovector effective masses. Moreover, under the assumption $|E| \ll mc^2$, the sound velocity v_s in nuclear matter can be obtained from the relation $mv_s^2 \approx K(\rho)/9$, and thus in symmetric nuclear matter, from Eqs. (28) and (30), one can also express the v_s in terms of Landau parameters as [52]

$$mv_s^2 \approx \frac{\hbar^2 k_F^2}{3m} \frac{1 + F_0}{1 + \frac{1}{3}F_1}. \quad (32)$$

For pure neutron matter, there are only four Landau parameters $F_l^{(n)}$ and $G_l^{(n)}$ ($l = 0, 1$). Similarly the conditions $G_0^{(n)} > -1$ and $G_1^{(n)} > -3$ guarantee the stability of pure neutron matter against spin polarization — or ferromagnetic transition. Explicit expressions for Landau parameters of pure neutron matter can be found in Ref. [23]. Generally, a critical density ρ_{cr} can be defined as the maximum density below which all the twelve Landau parameters of symmetric nuclear matter and pure neutron matter (except F_0 for symmetric nuclear matter at subsaturation density which leads to the well-known spinodal instability) satisfy the stability conditions.

For Skyrme interactions, as we pointed out before, to remove the spin and spin-isospin instabilities, one can omit the time-odd terms in $(\mathbf{s}_n + \mathbf{s}_p) \times (\mathbf{T}_n + \mathbf{T}_p)$ and $(\mathbf{s}_n - \mathbf{s}_p) \times (\mathbf{T}_n - \mathbf{T}_p)$, namely set $C_0^T = C_1^T = 0$ in the notation of Ref. [59]. It should be noted that, as mentioned in Ref. [51], with this prescription, the Landau parameters G_1 , G'_1 and $G_1^{(n)}$ all vanish, leading to unrealistic effective masses in polarized matter. In addition, if one

sets $C_0^T = C_1^T = 0$, the associated time-even terms in J^2 and J_q^2 also should be dropped for self-consistence. In the present work, we will impose $\rho_{cr} > 1.2 \text{ fm}^{-3}$ in the fitting procedure to construct the new parameter sets of the extended Skyrme interactions.

D. Isoscalar giant monopole resonance

The energy of the isoscalar giant monopole resonance — or the breathing mode — perhaps is the most important and efficient probe of the incompressibility of nuclear matter around ρ_0 . Thus we also include in our following fit the experimental data of the ISGMR energy for several spherical nuclei. The ISGMR energy is evaluated as

$$E_{\text{GMR}} = \sqrt{\frac{m_1}{m_{-1}}}, \quad (33)$$

where m_i are i -th energy weighted sum rules defined as

$$m_i = \sum_{\nu} |\langle \nu | \hat{F} | 0 \rangle|^2 (E_{\nu})^i. \quad (34)$$

Here $|\nu\rangle$ is the RPA excitation state for the monopole operator $\hat{F} = \sum_i^A r_i^2$.

It is well established that the energy weighted sum rule m_1 can be evaluated as [77]

$$m_1 = 2 \frac{\hbar^2}{m} A \langle r^2 \rangle, \quad (35)$$

where A is the nucleon number, m is the nucleon mass and $\langle r^2 \rangle$ is the ground-state rms radius. The moment m_{-1} can be calculated through the constrained-HF (CHF) approach [78, 79]

$$m_{-1} = - \frac{1}{2} \frac{d}{d\lambda} \langle \lambda | r^2 | \lambda \rangle^2 \Big|_{\lambda=0}, \quad (36)$$

where $|\lambda\rangle$ is the HF ground state for the CHF Hamiltonian $\hat{H} + \lambda \hat{F}$. In this work, we calculate the ISGMR energy using Eqs. (33), (35) and (36).

III. FITTING STRATEGY

In the present work, we use the simulated annealing method [64] to determine the parameters of the extended Skyrme interactions by minimizing the weighted sum of squared errors

$$\chi^2 = \sum_{i=1}^{N_d} \left(\frac{M_i^{\text{exp}} - M_i^{\text{th}}}{\sigma_i} \right)^2, \quad (37)$$

where N_d is the number of experimental data points, M_i^{exp} and M_i^{th} are the experimental and theoretical values for a selected observable, respectively, and σ_i is

the adopted error which is used to balance the relative weights of the various types of observables.

We include the following experimental data of a number of spherical even-even nuclei in the fit: (i) the binding energies E_B of 12 nuclei, namely, ^{16}O , $^{40,48}\text{Ca}$, $^{56,68}\text{Ni}$, ^{88}Sr , ^{90}Zr , $^{100,116,132}\text{Sn}$, ^{144}Sm , ^{208}Pb [80]; (ii) the charge rms radii r_c of 10 nuclei, namely, ^{16}O , $^{40,48}\text{Ca}$, ^{56}Ni , ^{88}Sr , ^{90}Zr , $^{116,132}\text{Sn}$, ^{144}Sm , ^{208}Pb [81, 82]; (iii) the ISGMR energies E_{GMR} of ^{90}Zr , ^{116}Sn , ^{144}Sm and ^{208}Pb [33]. To regulate the respective χ^2 for each sort of observable to be roughly equal to the number of corresponding data points, we assign a theoretical error 1.5 MeV to E_B , 0.015 fm to r_c while use the experimental error multiplied by a factor 3.54 for ISGMR energy E_{GMR} . In addition, the following constraints are considered in the optimization: (i) the critical density ρ_{cr} should be greater than 1.2 fm^{-3} ; (ii) the neutron $3p_{1/2} - 3p_{3/2}$ energy level splitting in ^{208}Pb should lie in the range of 0.8 – 1.0 MeV; (iii) the pressure of symmetric nuclear matter should be consistent with the constraints in the density region of $2\rho_0 < \rho < 4.6\rho_0$ obtained from analyzing flow data in heavy-ion collisions [36]; (iv) the EOS of pure neutron matter should conform to the predictions of the latest chiral effective field theory calculations with controlled uncertainties [14]. Furthermore, we fix the values of the magnitude $E_{\text{sym}}(\rho_c)$ and density slope $L(\rho_c)$ of the symmetry energy at $\rho_c = 0.11 \text{ fm}^{-3}$ to be equal to those extracted from the isotope binding energy difference [47] and the electric dipole polarizability in ^{208}Pb [83], i.e. $E_{\text{sym}}(\rho_c) = 26.65 \text{ MeV}$ and $L(\rho_c) = 47.3 \text{ MeV}$. For isoscalar and isovector effective masses at saturation density, $m_{s,0}^*$ and $m_{v,0}^*$, we consider three different cases: (i) $m_{s,0}^* = 0.9m$ and $m_{v,0}^* = 0.75m$ in parameter set eMSL09, which conform to the constraints we extracted recently from analyzing the giant resonances in ^{208}Pb [84]; (ii) $m_{s,0}^* = 0.8m$ and $m_{v,0}^* = 0.7m$ in parameter set eMSL08; (iii) $m_{s,0}^* = 0.7m$ and $m_{v,0}^* = 0.6m$ in parameter set eMSL07. For eMSL08 and eMSL07, the condition $m_{s,0}^* - m_{v,0}^* = 0.1m$ is imposed to be consistent with the extraction from global nucleon optical potentials constrained by world data on nucleon-nucleus and (p,n) charge-exchange reactions [85, 86].

IV. RESULTS AND DISCUSSIONS

Using the fitting procedure described in the previous section, we obtain three extended Skyrme interactions, namely, eMSL07, eMSL08 and eMSL09. Tab. I lists the values of the Skyrme parameters and the corresponding χ^2 . In the following, we discuss their performances in describing properties of spherical nuclei, nuclear matter and neutron stars. For comparison, we also show the corresponding results obtained with three typical interactions from Brussels group [27], i.e., BSk22, BSk24 and BSk26, which adopt the similar extended Skyrme interaction as in our present work and have been used to construct the HFB mass models. The BSk22 and

BSk24 parameter sets are adjusted to fit the EOS of neutron matter obtained by BHF calculations using Argonne V_{18} two-body force with compatible microscopic nuclear three-body forces [87], while BSk26 is adjusted to fit the well known Akmal-Pandharipande-Ravenhall (APR) EOS of neutron matter [9]. The symmetry energy value at saturation density is fixed at $E_{\text{sym}}(\rho_0) = 32$ MeV for BSk22 and at $E_{\text{sym}}(\rho_0) = 30$ MeV for both BSk24 and BSk26. In addition, the BSk family are also constrained to reproduce several properties of nuclear matter and to support the heaviest observed neutron stars [27]. For properties of finite nuclei, the BSk family are constructed based on Hartree-Fock-Bogoliubov (HFB) calculations with a microscopic pairing force and includes several additional corrections (e.g., the phenomenological Wigner terms and correction terms for the spurious collective energy) to better fit nuclear masses.

TABLE I: Skyrme parameters and χ^2 of the extended Skyrme parameter sets eMSL07, eMSL08 and eMSL09: lines 1–4 show the χ^2 evaluated from experimental data of binding energies, charge radii and ISGMR energies, namely $\chi_{E_B}^2$, $\chi_{r_c}^2$ and $\chi_{E_{\text{GMR}}}^2$, together with the total χ^2 , χ_{tot}^2 ; lines 5–18 show the Skyrme parameters. The last two lines show the calculated neutron skin thickness Δr_{np}^{208} and neutron $3p_{1/2} - 3p_{3/2}$ energy level splitting ϵ_{ls}^{208} of ^{208}Pb for the three interactions.

	eMSL07	eMSL08	eMSL09
χ_{tot}^2	24.48	23.45	22.68
$\chi_{E_B}^2$	13.47	10.07	8.25
$\chi_{r_c}^2$	7.16	9.17	10.17
$\chi_{E_{\text{GMR}}}^2$	3.85	4.22	4.26
$t_0(\text{MeV} \cdot \text{fm}^3)$	-2941.76	-2429.09	-2231.73
$t_1(\text{MeV} \cdot \text{fm}^5)$	575.338	493.720	431.073
$t_2(\text{MeV} \cdot \text{fm}^5)$	-398.554	-424.380	-426.692
$t_3(\text{MeV} \cdot \text{fm}^{3+3\alpha})$	16403.9	14502.7	14248.9
$t_4(\text{MeV} \cdot \text{fm}^{5+3\beta})$	-773.045	-724.215	-703.052
$t_5(\text{MeV} \cdot \text{fm}^{5+3\gamma})$	1159.83	887.873	668.913
x_0	0.371259	0.334701	0.280754
x_1	0.137412	0.132739	0.352663
x_2	-0.713811	-0.666437	-0.603887
x_3	0.412960	0.337131	0.177830
x_4	0.0852272	0.0754104	0.180194
x_5	-0.714565	-0.579724	-0.361533
α	0.132019	0.191960	0.231193
β	1	1	1
γ	1	1	1
$W_0(\text{MeV} \cdot \text{fm}^5)$	118.15	110.85	101.53
$\Delta r_{np}^{208}(\text{fm})$	0.182	0.183	0.183
$\epsilon_{ls}^{208}(\text{MeV})$	0.99	0.90	0.81

A. Properties of finite nuclei

In Fig. 1, we present the relative deviations of the binding energies and charge rms radii for a number of spherical nuclei calculated with the three new interactions eMSL07, eMSL08 and eMSL09 from the corresponding experimental data [80–82]. For the binding energy, we show the results for 41 spherical even-even nuclei for which the data are available, i.e., ^{16}O , ^{34}Si , ^{36}S , ^{38}Ar , $^{40,48}\text{Ca}$, ^{50}Ti , ^{52}Cr , ^{54}Fe , $^{56,68}\text{Ni}$, ^{84}Se , ^{86}Kr , ^{16}S , ^{18}Ar , ^{20}Ca , ^{22}Ti , ^{24}Cr , ^{26}Fe , ^{28}Ni , ^{34}Se , ^{36}Kr , ^{88}Sr , ^{90}Zr , ^{92}Mo , ^{94}Ru , ^{96}Pd , ^{98}Cd , $^{100,116,132}\text{Sn}$, ^{134}Te , ^{136}Xe , ^{138}Ba , ^{140}Zr , ^{142}Mo , ^{144}Ru , ^{146}Cd , ^{148}Sn , ^{150}Te , ^{152}Xe , ^{154}Ba , ^{156}Ce , ^{158}Nd , ^{160}Sm , ^{162}Gd , ^{164}Dy , ^{166}Er , ^{168}Yb , ^{170}Er , ^{172}Yb , ^{174}Hf , ^{176}Yb , ^{178}Hf , ^{180}Yb , ^{182}Hf , ^{184}Yb , ^{186}Hf , ^{188}Yb , ^{190}Hf , ^{192}Hf , ^{194}Hf , ^{196}Hf , $^{198,208,214}\text{Pb}$, ^{210}Po , ^{212}Rn , ^{214}Ra , ^{216}Th and ^{218}Pu ; for the charge rms radii, we show the results for 31 spherical even-even nuclei for which the data are available, i.e., ^{16}O , ^{36}S , ^{38}Ar , $^{40,48}\text{Ca}$, ^{50}Ti , ^{52}Cr , ^{54}Fe , ^{56}Ni , ^{86}Kr , ^{88}Sr , ^{90}Zr , ^{92}Mo , $^{116,132}\text{Sn}$, ^{136}Xe , ^{138}Ba , ^{140}Zr , ^{142}Mo , ^{144}Ru , ^{146}Cd , ^{148}Sn , ^{150}Te , ^{152}Xe , ^{154}Ba , ^{156}Ce , ^{158}Nd , ^{160}Sm , ^{162}Gd , ^{164}Dy , ^{166}Er , ^{168}Yb , ^{170}Er , ^{172}Yb , ^{174}Hf , ^{176}Yb , ^{178}Hf , ^{180}Yb , ^{182}Hf , ^{184}Yb , ^{186}Hf , ^{188}Yb , ^{190}Hf , ^{192}Hf , ^{194}Hf , ^{196}Hf , $^{198,208,214}\text{Pb}$, ^{210}Po , ^{212}Rn and ^{214}Ra . The hatched bands indicate a deviation within $\pm 1\%$. One can see that all the three new interactions can describe reasonably (within $\pm 1\%$) the ground-state properties of these spherical nuclei except for the light nucleus ^{16}O for which the deviations of charge rms radius are about 1.5%.

It should be noted that in the fitting, we use only 12 nuclei for the binding energy data and 10 nuclei for the charge rms radius data. The standard deviation for the binding energy of the fitted 12 nuclei is 1.59 MeV for eMSL07, 1.37 MeV for eMSL08, 1.24 MeV for eMSL09, and it becomes 1.043 MeV, 0.79 MeV and 1.018 MeV for BSk22, BSk24 and BSk26 [88], respectively. The standard deviation for the binding energy changes to 1.81 MeV for eMSL07, 1.63 MeV for eMSL08, 1.49 MeV for eMSL09, 0.66 MeV for BSk22, 0.56 MeV for BSk24, and 0.66 MeV for BSk26, for the 41 spherical even-even nuclei

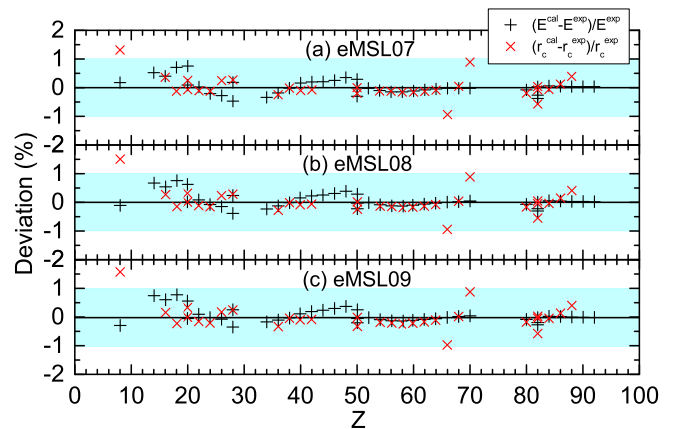


FIG. 1: (Color online) Deviations of the binding energies (plus symbols) and charge rms radii (cross symbols) of a number of nuclei with atomic number Z obtained from SHF calculations with eMSL07, eMSL08 and eMSL09 from those measured in experiments [80–82]. The bands indicate a deviation within $\pm 1\%$.

shown in Fig. 1. For the charge rms radius, the standard deviation of the fitted 10 nuclei is 0.0127 fm for eMSL07, 0.0144 fm for eMSL08, 0.0151 fm for eMSL09, while it becomes 0.0292 fm, 0.0255 fm and 0.0333 fm for BSk22, BSk24 and BSk26 [88], respectively. The standard deviation for the charge rms radius changes to 0.0162 fm for eMSL07, 0.0166 fm for eMSL08, 0.0169 fm for eMSL09, 0.0245 fm for BSk22, 0.0231 fm for BSk24, and 0.0290 fm for BSk26 for the 31 spherical even-even nuclei shown in Fig. 1. These results clearly indicate that the BSk family make a significant improvement on the description of the binding energy compared with the eMSL family, while the eMSL family give a better description of the charge rms radius, at least for the spherical even-even nuclei shown in Fig. 1.

We would also like to point out that, in our fits and calculations, the pairing effects are treated within the framework of BCS theory with the constant gap approximation. This treatment of the pairing should be reasonable for the fitted nuclei in the present work since they are essentially (semi-)doubly magic nuclei for which the pairing effects are unimportant. For the nuclei with neutron or proton number deviating from magic number, the pairing effects might be important, and the more sophisticated Bogoliubov treatment with a microscopic pairing force as well as some additional corrections, such as the Wigner terms and the spurious collective energy, can better reproduce the binding energy over the whole nuclear chart as demonstrated in the HFB calculations (see e.g. Ref. [22, 23, 27, 30] and references therein). Therefore, while the present eMSL family can reasonably describe the binding energies and charge rms radii of the ground-state spherical even-even nuclei, using the more sophisticated treatment of the pairing effects and including some additional corrections (e.g., the Wigner terms and the spurious collective energy) are important to improve the description of the binding energy over the whole nuclear chart. In addition, in the present work, we only focus on the spherical nuclei without considering nuclear deformation which should be important for the description of nuclei in the whole nuclear chart. Nevertheless, a very accurate description of the binding energy over the whole nuclear chart is beyond the scope of the present work and this could be pursued in future.

Furthermore, the first three rows in Tab. I show that the variation of the effective masses has little impact on the fitting quality for the data of the binding energies and charge radii. Moreover, the χ^2 for the binding energy and charge radius calculated with the three interactions (see Table I) suggest that the binding energy data prefer a larger $m_{s,0}^*$ while the charge radius data favor a smaller $m_{s,0}^*$, and these features are consistent with the results in the SHF model with the standard Skyrme interactions [89].

The neutron skin thickness $\Delta r_{np} = \langle r_n^2 \rangle^{1/2} - \langle r_p^2 \rangle^{1/2}$, i.e., the difference of the neutron and proton rms radii, is of particular importance for the study of the density dependence of the symmetry energy. Mean field calcula-

tions using many different relativistic and nonrelativistic interactions have indicated that the neutron skin thickness is strongly correlated to the density slope $L(\rho_0)$ of the symmetry energy at saturations density [90–92]. Moreover, in Ref. [47], we find the neutron skin thickness of heavy nuclei is uniquely determined by $L(\rho_c)$ at a subsaturation density $\rho_c = 0.11 \text{ fm}^{-3}$. So we show in row 19 of Tab. I the neutron skin thickness of ^{208}Pb , Δr_{np}^{208} , predicted by HF calculations using the three new interactions. Due to the imposed condition $L(\rho_c) = 47.3 \text{ MeV}$, the eMSL family predict quite similar values of Δr_{np}^{208} , i.e., about 0.18 fm, which are in very good agreement with the $\Delta r_{np}^{208} = 0.170 \pm 0.016 \text{ fm}$ and $\Delta r_{np}^{208} = 0.176 \pm 0.027 \text{ fm}$ obtained, respectively, from SHF analyses of neutron skin data of Sn isotopes [47] and experimental data of the electric dipole polarizability α_D in ^{208}Pb [83]. These results are also consistent with the estimated range $\Delta r_{np}^{208} = 0.165 \pm (0.009)_{\text{expt}} \pm (0.013)_{\text{theor}} \pm (0.021)_{\text{est}} \text{ fm}$ extracted from the measured α_D in ^{208}Pb [93], the constraint $\Delta r_{np}^{208} = 0.15 \pm 0.03(\text{stat.})_{-0.03}^{+0.01}(\text{sys.}) \text{ fm}$ from coherent pion photoproduction cross sections [94], and the constraint $\Delta r_{np}^{208} = 0.33_{-0.18}^{+0.16} \text{ fm}$ extracted from PREX at JLab [95]. We note that the BSk22 predicts a neutron skin thickness of ^{208}Pb , i.e., $\Delta r_{np}^{208} = 0.18 \text{ fm}$ [27], while both BSk24 and BSk26 predict a little smaller value of $\Delta r_{np}^{208} = 0.14 \text{ fm}$ [27]. This feature can be understood from the fact that the Δr_{np}^{208} is uniquely determined by $L(\rho_c)$ at a subsaturation density $\rho_c = 0.11 \text{ fm}^{-3}$ [47], and both BSk24 and BSk26 have a smaller value of $L(\rho_c) = 38.1 \text{ MeV}$ while BSk22 has a value of $L(\rho_c) = 49.3 \text{ MeV}$ (see Table III in the following).

The single-particle spectra are also important observables and have profound impacts on the properties of super-heavy nuclei [96]. However, it is known that the HF approach can not well describe the single-particle energies due to the self-interaction error [15], and thus we have not included them in our present fit. Unlike the single-particle energies, their differences among particle states or hole states (e.g., the spin-orbit splitting without crossing the shell gap), are believed to be robust observables which can be safely compared with the results of HF calculations [15]. Here we list in last row of Tab. I the neutron $3p_{1/2} - 3p_{3/2}$ energy level splitting in ^{208}Pb , $\epsilon_{l_s}^{208}$, for the eMSL family. As one can see, the results, especially $\epsilon_{l_s}^{208} = 0.90 \text{ MeV}$ for eMSL08, well agree with

TABLE II: Comparison of the ISGMR energies $E_{\text{GMR}} = \sqrt{m_1/m_{-1}}$ (in MeV) in ^{90}Zr , ^{116}Sn , ^{144}Sm and ^{208}Pb obtained for the eMSL07, eMSL08 and eMSL09 interactions with the experimental data [33–35].

Nucleus	TAMU	RCNP	eMSL07	eMSL08	eMSL09
^{90}Zr	17.81 ± 0.35	—	17.65	17.68	17.70
^{116}Sn	15.90 ± 0.07	15.70 ± 0.10	16.19	16.20	16.21
^{144}Sm	15.25 ± 0.11	—	15.28	15.27	15.29
^{208}Pb	14.18 ± 0.11	13.50 ± 0.10	13.57	13.53	13.54

the experimental value 0.89 MeV [17].

For the ISGMR energy, we show in Tab. II the calculated results together with the corresponding experimental data reported by TAMU group [33] and RCNP group [34, 35]. It can be seen that the three new interactions predict very similar and overall reasonable monopole response properties.

B. Properties of nuclear matter

In this subsection we discuss the properties of infinite nuclear matter predicted by the three new extended Skyrme interactions. We present in Tab. III the values of a number of macroscopic quantities in the SHF model with MSL07, eMSL08 and eMSL09. The corresponding results with the BSk22, BSk24 and BSk26 interactions [27] are also included in Tab. III for comparison. One can see that the eMSL family predict very similar and reasonable macroscopic quantities at saturation density. In particular, the values of the magnitude and density slope of the symmetry energy, $E_{\text{sym}}(\rho_0)$ and $L(\rho_0)$, are essentially consistent with other constraints obtained from analyzing terrestrial experiments and astrophysical observations as well as the predictions of theoretical calculations [14, 97–100]. The calculated results of higher-order coefficients J_0 and $K_{\text{sym}}(\rho_0)$ with the eMSL family are also in very good agreement with their empirical values [67, 69, 70]. Compared with the eMSL family, the BSk family give larger K_0 and J_0 , and thus predict stiffer EOSs of SNM, especially at high densities, which may have considerable effects on neutron star properties. Moreover, the BSk family predict rather different values of isovector macroscopic quantities $L(\rho_0)$ and $K_{\text{sym}}(\rho_0)$ which suggests they lead to very different density dependence of the symmetry energy especially in high-density region. In the following, we will give a more detailed discussion on the EOSs obtained with the six extended Skyrme interactions.

In the last row of Tab. III, we also show the values of the second-order symmetry coefficient $K_{\text{sat},2} = K_{\text{sym}} - (6 + J_0/K_0)L$ for the isobaric incompressibility of asymmetric nuclear matter [67], for the six extended Skyrme interactions. It is generally believed that the coefficient $K_{\text{sat},2}$ can be extracted from the ISGMR energy E_{GMR} of neutron-rich nuclei which is related to the incompressibility of finite nuclei, K_A , through the relation [101]

$$E_{\text{GMR}} = \sqrt{\frac{\hbar^2}{m\langle r^2 \rangle}} K_A. \quad (38)$$

In the leptodermous approximation, K_A can be expressed as [101]

$$K_A = K_v + K_s A^{-1/3} + K_\tau \left(\frac{N-Z}{A} \right)^2 + K_c \frac{Z^2}{A^{4/3}} \quad (39)$$

with K_v , K_s , K_τ , K_c being the volume, surface, isospin and Coulomb terms, respectively. Here high order terms in powers of $A^{1/3}$ and $(N-Z)/A$ are neglected, and the K_τ parameter is usually thought to be equivalent to the $K_{\text{sat},2}$ parameter. By fitting ISGMR energies of Sn and Cd isotopes using the above formula, Li *et al.* and Patel *et al.* obtained $K_\tau = -550 \pm 100$ MeV and $K_\tau = -555 \pm 75$ MeV, respectively [34, 102, 103]. And a recent analysis of the ISGMR experimental data by Stone *et al.* leads to a constraint of $-840 < K_\tau < -350$ MeV with a large uncertainty [104]. The magnitudes of these constrained K_τ are essentially larger than those of $K_{\text{sat},2}$ predicted by the three new interactions as well as the BSk interactions. At this point, it should be pointed out that, since the extracted values of K_τ are contaminated by contributions of high-order terms which are neglected in Eq. (39), one should not directly compare them against the value of $K_{\text{sat},2}$ from the SHF calculations [104, 105]. From Tab. III, one can see that while the eMSL family predict similar $K_{\text{sat},2}$, the BSk family, especially BSk24, predict larger values of $K_{\text{sat},2}$. It is interesting to see that the predictions of both eMSL family and BSk family are all in very good agreement with the estimated value of $K_{\text{sat},2} = -370 \pm 120$ MeV obtained from a standard SHF model [67] analysis on the symmetry energy constrained in heavy-ion collisions [50, 106]. To date the accurate determination of $K_{\text{sat},2}$ remains an open challenge.

To see more clearly the nuclear matter properties, we show in Fig. 2 the pressure of symmetric nuclear matter $P_{\text{SNM}}(\rho)$, the binding energy per neutron in pure neutron matter $E_{\text{PNM}}(\rho)$ and the symmetry energy $E_{\text{sym}}(\rho)$ as functions of densities for eMSL07, eMSL08, eMSL09, BSk22, BSk24 and BSk26. For comparison, Fig. 2 also includes the constraints on $P_{\text{SNM}}(\rho)$ in the density region of $2\rho_0$ – $4.6\rho_0$ from analyzing the flow data in relativistic heavy-ion collisions (Flow Data) [36]; the predictions on $E_{\text{PNM}}(\rho)$ at subsaturation densities from ChEFT calculations using next-to-next-to-next-to-leading order (N3LO) potential (ChEFT) [14]; the constraints on the density dependence of the symmetry energy at subsaturation densities from transport model analyses of mid-peripheral heavy-ion collisions of Sn isotopes (HIC) [50] and the SHF analyses of isobaric analog states (IAS) as well as combining additionally the neutron skin data (IAS+NSkin) [46]. In addition, the constraints (α_{D} in ^{208}Pb) on $E_{\text{PNM}}(\rho)$ and $E_{\text{sym}}(\rho)$ extracted recently from analyzing the electric dipole polarizability α_{D} in ^{208}Pb [49] are also displayed in Fig. 2 (b) and (c), respectively. It can be seen that, compared with the BSk interactions, the eMSL family predict relatively softer EOSs of SNM at supra-saturation densities while stiffer symmetry energies at subsaturation densities. We also notice that the eMSL family predict very similar symmetric nuclear matter properties even up to $5\rho_0$ as well as almost the same pure neutron matter EOS and the density dependence of the symmetry energy at subsaturation densities. As we mentioned before, the EOS of symmetric nuclear matter can be well constrained by the proper-

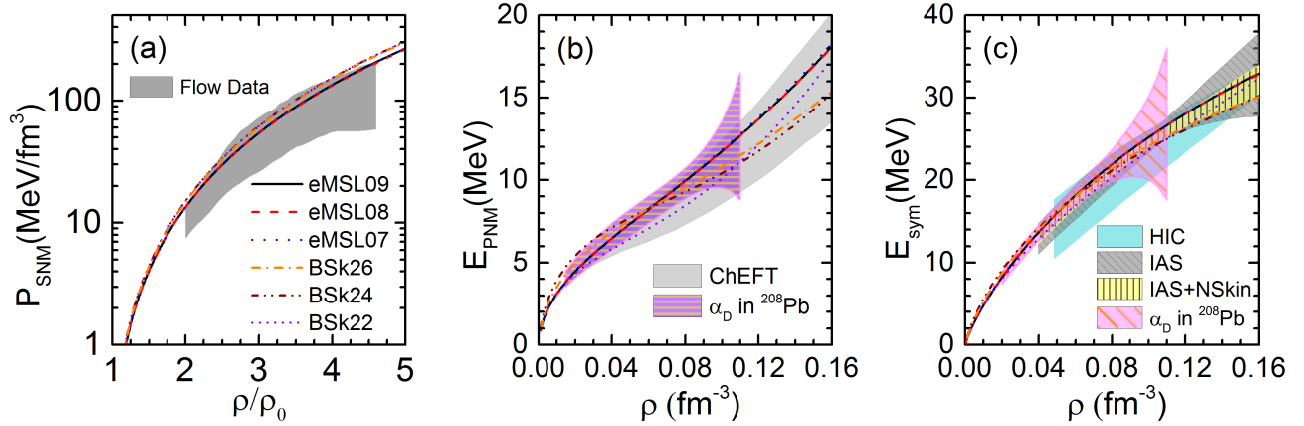


FIG. 2: (Color online) Pressure of symmetric nuclear matter $P_{\text{SNM}}(\rho)$ (a), the binding energy per nucleon of pure neutron matter $E_{\text{PNM}}(\rho)$ (b) and the symmetry energy $E_{\text{sym}}(\rho)$ (c) as functions of densities obtained from HF calculations using eMSL07, eMSL08, eMSL09, BSk22, BSk24 and BSk26. Several constraints from analyzing experimental data and the predictions of theoretical calculations are also included for comparison (see text for the details).

TABLE III: Macroscopic quantities in the SHF model with eMSL07, eMSL08 and eMSL09. The corresponding results from BSk22, BSk24, and BSk26 [27] are also included for comparison

	eMSL07	eMSL08	eMSL09	BSk22	BSk24	BSk26
$\rho_0(\text{fm}^{-3})$	0.1584	0.1584	0.1583	0.1578	0.1578	0.1589
$E_0(\rho_0)(\text{MeV})$	-16.043	-16.040	-16.034	-16.088	-16.048	-16.064
$K_0(\text{MeV})$	229.7	229.0	229.6	245.9	245.5	240.8
$J_0(\text{MeV})$	-339.9	-351.4	-352.7	-275.5	-274.5	-282.9
$E_{\text{sym}}(\rho_c)(\text{MeV})$	26.65	26.65	26.65	25.03	24.98	25.3
$L(\rho_c)(\text{MeV})$	47.3	47.3	47.3	49.3	38.1	38.1
$K_{\text{sym}}(\rho_c)(\text{MeV})$	-94.7	-92.7	-91.1	-32.5	-67.3	-103.5
$G_S(\text{MeV}\cdot\text{fm}^5)$	118.8	104.2	92.8	116.6	113.4	118.6
$G_V(\text{MeV}\cdot\text{fm}^5)$	58.2	49.9	58.4	21.2	20.2	38.2
$G_{SV}(\text{MeV}\cdot\text{fm}^5)$	-9.0	-8.3	-9.5	-6.2	-6.2	3.83
$G'_0(\rho_0)$	0.24	0.19	0.17	0.39	0.40	0.41
$m_{s,0}^*/m$	0.7	0.8	0.9	0.80	0.80	0.80
$m_{v,0}^*/m$	0.6	0.7	0.75	0.71	0.71	0.65
$E_{\text{sym}}(\rho_0)(\text{MeV})$	32.7	32.8	32.8	32.0	30.0	30.0
$L(\rho_0)(\text{MeV})$	52.1	53.0	53.9	68.5	46.4	37.5
$K_{\text{sym}}(\rho_0)(\text{MeV})$	-125.1	-111.9	-96.7	13.0	-37.6	-135.6
$K_{\text{sat},2}(\text{MeV})$	-360.4	-348.8	-337.2	-321.2	-264.0	-316.6

ties of finite nuclei and experimental data of heavy-ion collisions. It is not surprising to see that the three new extended Skyrme interactions predict almost the same $E_{\text{PNM}}(\rho)$ and $E_{\text{sym}}(\rho)$ at subsaturation densities, as the magnitude and density slope of the symmetry energy at $\rho_c = 0.11 \text{ fm}^{-3}$, namely $E_{\text{sym}}(\rho_c)$ and $L(\rho_c)$, are imposed to be 26.65 MeV and 47.3 MeV, respectively. This condition guarantees the eMSL family predict reasonable density dependence of the symmetry energy or the EOS of asymmetric nuclear matter below and around ρ_0 .

Overall, for the properties of nuclear matter below and around saturation density, the eMSL and BSk family give quite similar predictions. The eMSL family make a small

improvement on the supra-saturation density behaviors of symmetric nuclear matter for which the BSk interactions predict a little too large pressure around $2\rho_0$ and above $4\rho_0$ compared with the constraint from flow data in heavy-ion collisions [36], as shown in Fig. 2 (a). In addition, the EOSs of pure neutron matter given by the eMSL family are in better agreement with the recent constraint obtained from analyzing the α_D data of ^{208}Pb [49] as well as the predictions from the recent ChEFT calculations using N3LO potential [14], as shown in Fig. 2 (b).

For high-density behaviors of the symmetry energy, we exhibit in the upper panel of Fig. 3 the symmetry energy $E_{\text{sym}}(\rho)$ as a function of density up to 1 fm^{-3} for the

eMSL and BSk family. One can see that all these extended Skyrme interactions except BSk26 predict a soft symmetry energy below and around saturation density but a stiff symmetry energy at supra-saturation densities. For the BSk26 interaction, the symmetry energy almost remains constant in the density region of $\rho > 2\rho_0$. In addition, the eMSL09 and BSk24 interactions predict very similar high-density behaviors of the symmetry energy. It is interesting to see that the symmetry energy predictions from the eMSL family are consistent with the constraint from very low density to $3\rho_0$ obtained recently by extrapolating the well constrained subsaturation density symmetry energy based on systematics of various relativistic and nonrelativistic EDFs [107]. Given the present poor knowledge on the high-density behaviors of the symmetry energy, we show in the lower panel of Fig. 3 the comparison of the pure neutron matter EOS $E_{\text{PNM}}(\rho)$ as a function of density ρ for the eMSL and BSk family with the predictions of nonrelativistic BHF calculations using realistic Argonne V_{18} force together with compatible microscopic three-body forces [87] and the well known APR EOS using the realistic $A18+\delta v + \text{UIX}^*$ interaction [9]. One can see that the extended Skyrme interactions predict very reasonable neutron matter EOSs that are consistent with the microscopic calculations. In particular, the EOS of pure neutron matter with eMSL09 is very close to that with BSk24 as well as the BHF cal-

culations, while those with eMSL07 and eMSL08 lie between the APR and BHF EOSs.

We would like to emphasize that the main difference of nuclear matter properties for the three new extended Skyrme interactions is the high-density behaviors of the EOS of asymmetric nuclear matter or the symmetry energy. This is partly because of the variation of $m_{s,0}^*$ and $m_{v,0}^*$ values in these extended Skyrme interactions, which has essential impacts on the \mathcal{H}_{eff} (i.e., Eq. (6)) and is related to the momentum dependence of the three body forces. Therefore, the additional momentum and density dependent two-body forces which effectively simulate the momentum dependence of the three-body force may play an important role for the high-density behaviors of the EOS of asymmetric nuclear matter. The three new extended Skyrme interactions constructed in the present work predict very similar properties of nuclear matter below and around saturation density but different high-density behaviors of the symmetry energy, and thus are potentially useful for the investigation of the currently largely uncertain high-density behaviors of the symmetry energy.

C. Landau parameters

We calculate the density dependence of the Landau parameters of symmetric nuclear matter and pure neutron matter according to the explicit expressions in Refs. [22, 23] with the eMSL and BSk family, and the results are exhibited in Fig. 4 and Fig. 5, respectively. One can see that for the three new extended Skyrme interactions, all the Landau parameters, except F_0 for symmetric nuclear matter, satisfy the stability conditions at densities up to 1.2 fm^{-3} and thus guarantee the stability of symmetric nuclear matter and pure neutron matter from subsaturation densities to very high densities. The instability of symmetric nuclear matter at densities below about 0.1 fm^{-3} determined by the value of F_0 corresponds to the well-known spinodal instability, which is physical and is believed to be related to the liquid-gas phase transition in nuclear matter and the multifragmentation phenomenon observed in heavy-ion collisions at intermediate energies [108, 109]. In the spinodal instability region of symmetric nuclear matter, the squared sound velocity or the incompressibility of symmetric nuclear matter is negative (see, e.g., Eq. (32) and the relation $mv_s^2 \approx K(\rho)/9$). At densities beyond 1.2 fm^{-3} , both symmetric nuclear matter and pure neutron matter become unstable in the spin-isospin channels, and the density $\rho = 1.2 \text{ fm}^{-3}$ is thus the critical density for the eMSL interactions. For BSk24 and BSk26 interactions, these instabilities are eliminated at even higher densities. For the interaction BSk22, the instabilities are also eliminated at very higher densities except that the ferromagnetic instability in pure neutron matter will appear in the density region from 0.34 fm^{-3} to 1.02 fm^{-3} where one has $G_0^{(n)} < -1$. The large value of 1.2 fm^{-3} of

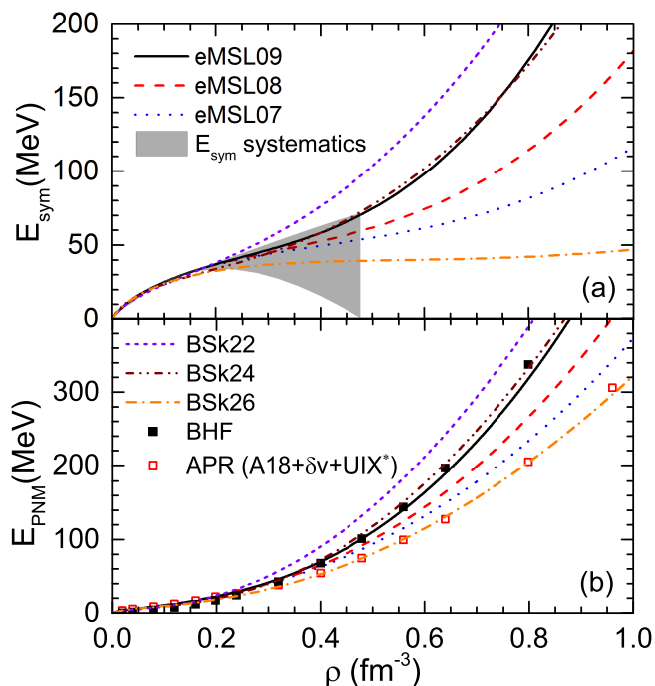


FIG. 3: (Color online) Density dependence of the symmetry energy $E_{\text{sym}}(\rho)$ (a) and EOSs of pure neutron matter $E_{\text{PNM}}(\rho)$ (b) for the extended Skyrme interactions eMSL07, eMSL08, eMSL09, BSk22, BSk24 and BSk26. The shaded band in panel (a) is taken from Ref. [107]. The $E_{\text{PNM}}(\rho)$ of APR is taken from Ref. [9] while that of BHF is from Ref. [87].

the critical density ensures that the three new extended Skyrme interactions obtained in the present work can be used safely to calculate the structure of neutron stars. As we will see later, the center densities of the neutron stars with largest mass configuration obtained with eMSL07, eMSL08 and eMSL09 are all less than $\rho = 1.2 \text{ fm}^{-3}$.

To close this subsection, we list in Tab. IV the values of all the twelve Landau parameters of symmetric nuclear matter and pure neutron matter at saturation density in the SHF model with the eMSL and BSk family.

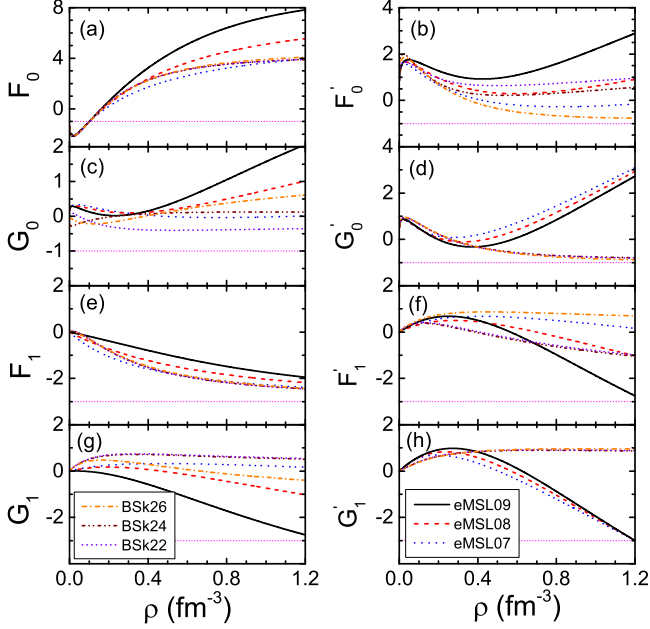


FIG. 4: (Color online) Density dependence of the Landau parameters of symmetric nuclear matter for the extended Skyrme interactions eMSL07, eMSL08, eMSL09, BSk22, BSk24 and BSk26. The short-dash-dotted lines indicate the critical stability conditions.

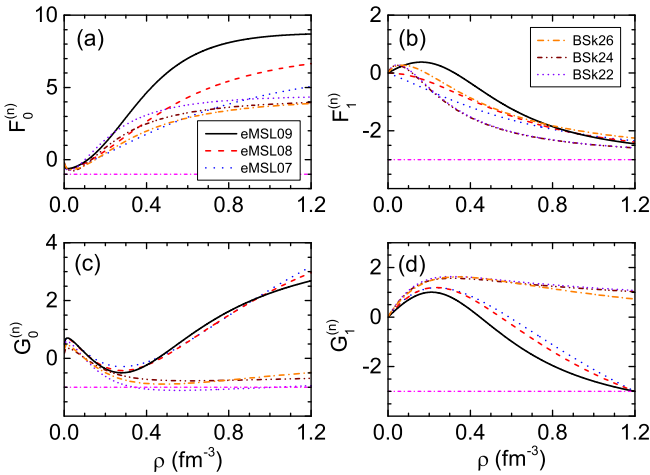


FIG. 5: (Color online) Similar to Fig. 4 but for pure neutron matter.

TABLE IV: Landau parameters of symmetric nuclear matter and pure neutron matter at saturation density in the SHF model with eMSL07, eMSL08, eMSL09, BSk22, BSk24 and BSk26.

	eMSL07	eMSL08	eMSL09	BSk22	BSk24	BSk26
F_0	-0.27	-0.17	-0.06	-0.10	-0.10	-0.12
F'_0	0.88	1.15	1.42	1.10	0.97	0.96
F_1	-0.90	-0.60	-0.30	-0.60	-0.60	-0.60
F'_1	0.50	0.43	0.60	0.40	0.37	0.67
G_0	0.21	0.16	0.05	-0.24	-0.061	-0.21
G'_0	0.24	0.19	0.17	0.39	0.40	0.41
G_1	0.22	0.17	-0.08	0.64	0.63	0.48
G'_1	0.67	0.76	0.83	0.56	0.55	0.54
$F_0^{(n)}$	0.09	0.23	0.54	0.83	0.32	-0.074
$F_1^{(n)}$	-0.48	-0.20	0.37	-0.23	-0.27	-0.094
$G_0^{(n)}$	-0.06	-0.14	-0.17	-0.41	-0.26	-0.32
$G_1^{(n)}$	1.07	1.08	0.93	1.40	1.34	1.31

D. Neutron star properties

In the following, we discuss the mass-radius relation of static neutron stars, which is obtained by solving the famous Tolman-Oppenheimer-Volkov (TOV) equation [110, 111], i.e.,

$$\frac{dP(r)}{dr} = -\frac{G}{c^2 r^2} \left[\epsilon(r) + \frac{P(r)}{c^2} \right] \times \left[M(r) + 4\pi r^3 \frac{P(r)}{c^2} \right] \left[1 - \frac{2GM(r)}{c^2 r} \right]^{-1} \quad (40)$$

$$\frac{dM(r)}{dr} = 4\pi \epsilon(r) r^2 / c^2, \quad (41)$$

where r is the radial coordinate, $M(r)$ is the gravitational mass inside the sphere of radius r , $\epsilon(r)$ and $P(r)$ are, respectively, the corresponding energy density and pressure of the neutron star matter at r , and G is Newton's gravitational constant,

To solve the TOV equation, an EOS of neutron star matter $P(\epsilon)$ is necessary. In the present work, we assume the core of neutron stars consists of neutron, proton, electrons and possible muons without phase transition and other degrees of freedom at high densities. Then the EOS of neutron star matter is constructed in the following way: for the core, we calculate the EOS of $npe\mu$ matter in SHF model using the extended Skyrme interactions; for the outer crust, we use the EOS of BPS (FMT) in the region of $6.93 \times 10^{-13} \text{ fm}^{-3} < \rho < \rho_{\text{out}}$ ($4.73 \times 10^{-15} \text{ fm}^{-3} < \rho < 6.93 \times 10^{-13} \text{ fm}^{-3}$) [112]; for the inner crust in the density region between ρ_{out} and ρ_t we construct its EOS by interpolation with the form [113, 114]

$$P = a + b\epsilon^{4/3}. \quad (42)$$

In this work, the critical density between the inner and the outer crust is taken to be $\rho_{\text{out}} = 2.46 \times$

TABLE V: Maximum mass of the neutron star (M_{\max}), the center density of the maximum mass neutron star configuration (ρ_{\max}^{cen}), the radius of $1.4M_{\odot}$ neutron star ($R_{1.4}$), and core-crust transition density of the neutron star (ρ_t) for eMSL07, eMSL08, eMSL09, BSk22, BSk24 and BSk26.

	eMSL07	eMSL08	eMSL09	BSk22	BSk24	BSk26
M_{\max}/M_{\odot}	2.17	2.19	2.21	2.27	2.28	2.17
ρ_{\max}^{cen} (fm^{-3})	1.11	1.06	1.03	0.98	0.98	1.13
$R_{1.4}$ (km)	12.3	12.5	12.7	13.2	12.5	11.8
ρ_t (fm^{-3})	0.076	0.077	0.078	0.071	0.080	0.085

10^{-4} fm^{-3} [113, 114], and ρ_t is the core-crust transition density which is evaluated self-consistently using the extended Skyrme interactions within the thermodynamic

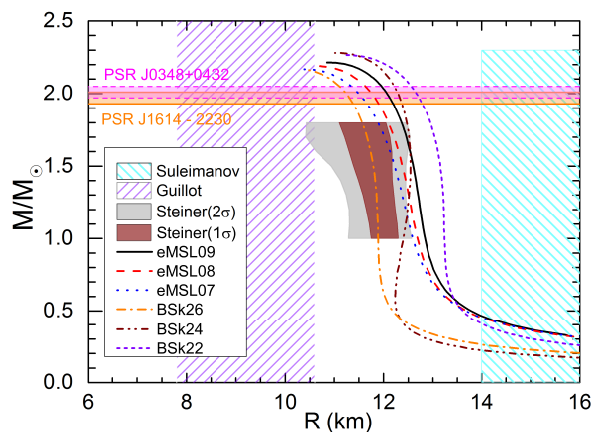


FIG. 6: (Color online) Mass-radius relation of neutron stars obtained with eMSL07, eMSL08, eMSL09, BSk22, BSk24 and BSk26. Some recent observational constraints [31, 32, 115–117] are also included for comparison (see text for the details).

We present in Tab. V the maximum mass M_{\max} , the center density ρ_{\max}^{cen} of the maximum mass neutron star configuration, the radius of $1.4M_{\odot}$ neutron star $R_{1.4}$ and the core-crust transition density ρ_t for eMSL07, eMSL08, eMSL09, BSk22, BSk24 and BSk26 [27]. It can be seen that all the six extended Skyrme interactions can successfully support $2M_{\odot}$ neutron stars. From the results of the eMSL family, one can find that the interaction with a stiffer symmetry energy at high-density region predicts a larger maximum mass and a larger stellar radius for a canonical neutron star with mass of $1.4M_{\odot}$. In addition, as mentioned earlier, the values of ρ_{\max}^{cen} for the three new extended Skyrme interactions are all less than the critical density of $\rho_{\text{cr}} = 1.2 \text{ fm}^{-3}$. For the core-crust transition density ρ_t , which is strongly correlated with $L(\rho_c)$ or $L(\rho_0)$ [68, 83], the eMSL interactions also produce very similar values that are consistent with the empirical value [1] as well as the result with BSk interactions.

Shown in Fig. 6 is the mass-radius relation of static neutron stars obtained with eMSL09, eMSL08, eMSL07,

BSk22, BSk24 and BSk26 [27]. It is interesting to see that the BSk24 interaction predicts smaller radii for low-mass neutron stars while larger radii for high-mass neutron stars. This could be due to the fact that the BSk24 interaction predicts a softer symmetry energy around saturation density while stiffer SNM EOS and symmetry energy at supra-saturation densities. The horizontal bands in Fig. 6 indicate the measured masses $M = 1.97 \pm 0.04M_{\odot}$ [31] and $M = 2.01 \pm 0.04M_{\odot}$ [32] of the two heaviest neutron stars PSR J1614-2230 [31] and PSR J0348+0432 [32], respectively. For comparison, we also show in Fig. 6 the constraints on the radii of neutron stars by Steiner *et al.* from analyses of three X-ray bursters and three transient low-mass X-ray binaries [115]. It should be noted that, by analyzing the same data sets using more sophisticated atmosphere models, Suleimanov *et al.* concluded that the lower limit on the stellar radius is 14 km for masses below $2.3M_{\odot}$ [116], which is included in Fig. 6 for comparison. Indeed, large systematic uncertainties in the analysis of X-ray bursters have hindered the reliability of these results. Another way to extract the radii of neutron stars is from the observation of quiescent low mass X-ray binaries (qLMXB) in globular clusters. By assuming the neutron star radius is independent on mass, namely $R(M) = R_0$, Guillot *et al.* [117] determined a rather small stellar radius of $R_0 = 9.1_{-1.5}^{+1.3} \text{ km}$ within 90% confidence level from fitting the spectra of five qLMXBs, which is also displayed in Fig. 6 for comparison. Note that the assumption $R(M) = R_0$ is rather strong and the additional conditions of causality together with $2M_{\odot}$ neutron stars may change the result [118]. Therefore, the accurate determination of the radius of neutron stars, which can put a stringent constraint on the density dependence of the symmetry energy beyond saturation density [119], is still a big challenge. The radii of the $1.4M_{\odot}$ neutron star ($\sim 12.5 \text{ km}$) predicted by the eMSL family are in very good agreement with recent studies based on nuclear experiments and theoretical calculations of pure neutron matter (see, e.g., Ref. [118] and references therein).

V. CONCLUSIONS

Within the framework of the extended Skyrme interaction which includes additional momentum and density dependent terms to simulate the momentum dependence of three-body nuclear force, we have constructed three new extended Skyrme interactions, namely, eMSL07, eMSL08 and eMSL09, by fitting experimental data of a number of finite nuclei together with a few additional constraints on nuclear matter with the simulated annealing method. We have shown that the eMSL family of extended Skyrme interactions can reasonably describe the ground-state properties and the isoscalar giant monopole resonance energies of various spherical nuclei used in the fit as well as the ground-state properties of many other spherical nuclei, and conform to various most recent con-

straints on nuclear matter EOS from theory, experiment and observation. The high-density EOSs of pure neutron matter for the three new extended Skyrme interactions are also consistent with the predictions of the microscopic calculations using realistic nuclear forces. Moreover, the three new extended Skyrme interactions successfully eliminate the unphysical instabilities in nuclear matter at densities up to about $7.5\rho_0$, and so the eMSL family constructed in the present work are suitable for the study of neutron stars. We have used the three new extended Skyrme interactions to study the mass-radius relation of neutron stars and our results indicate that the eMSL family can support $2M_\odot$ neutron stars and predict very reasonable stellar radii.

We have also made comparison for the predictions of finite nuclei, nuclear matter and neutron stars with the three new eMSL interactions versus those with the accurately calibrated interactions BSk22, BSk24 and BSk26. Although obtained through very different fitting strategies, the new eMSL interactions and BSk interactions give quite similar predictions for nuclear matter and neutron stars with the main difference appeared for some higher-order characteristic parameters of asymmetric nuclear matter, e.g., J_0 , L , K_{sym} , and $K_{\text{sat},2}$. For finite nuclei, while the present eMSL family in Hartree-Fock calculations with the BCS pairing framework under the constant gap approximation can reasonably describe the binding energies and charge rms radii of the ground-state spherical even-even nuclei as well as the isoscalar giant monopole resonance energies of several representative finite nuclei, we have noted that the more sophisticated Bogoliubov treatment for pairing effects with a microscopic pairing force as well as some additional corrections, such as the Wigner terms and the spurious collective energy, can significantly improve the description of the binding energy over the whole nuclear chart as demonstrated in the Hartree-Fock-Bogoliubov calculations with BSk22, BSk24 and BSk26. We would like to point out that a very accurate nuclear mass model over the whole nuclear chart is beyond the scope of the present work and perhaps this could be pursued in future.

In conclusion, by including the additional momentum and density dependent two-body terms in the Skyrme interaction, which effectively simulate the momentum dependence of three-body nuclear force, we have constructed three new extended Skyrme interactions, namely, eMSL07, eMSL08 and eMSL09, which can simultaneously well describe nuclear matter, finite nuclei and neutron stars. The three new eMSL interactions predict very similar properties of finite nuclei and nuclear matter below and around saturation density but different high-density behaviors of the symmetry energy, and thus they are potentially useful for the study of the currently largely uncertain high-density symmetry energy.

Acknowledgments

This work was supported in part by the Major State Basic Research Development Program (973 Program) in China under Contract Nos. 2013CB834405 and 2015CB856904, the NNSF of China under Grant Nos. 11625521, 11275125 and 11135011, the ‘‘Shu Guang’’ project supported by Shanghai Municipal Education Commission and Shanghai Education Development Foundation, the Program for Professor of Special Appointment (Eastern Scholar) at Shanghai Institutions of Higher Learning, and the Science and Technology Commission of Shanghai Municipality (11DZ2260700).

Appendix A: Macroscopic quantities in the extended SHF model

In the SHF model with the extended Skyrme interaction given in Eqs. (1) and (2), the EOS of asymmetric nuclear matter can be expressed as [22]

$$\begin{aligned}
 E(\rho, \delta) = & \frac{3\hbar^2}{10m}k_F^2F_{5/3} \\
 & + \frac{1}{8}t_0\rho[2(x_0+2) - (2x_0+1)F_2] \\
 & + \frac{1}{48}t_3\rho^{\alpha+1}[2(x_3+2) - (2x_3+1)F_2] \\
 & + \frac{3}{40}\rho k_F^2\left\{[t_1(x_1+2) + t_2(x_2+2)]F_{5/3} \right. \\
 & \left. + \frac{1}{2}[t_2(2x_2+1) - t_1(2x_1+1)]F_{8/3}\right\} \\
 & + \frac{3}{40}\rho k_F^2\left\{[t_4(x_4+2)\rho^\beta + t_5(x_5+2)\rho^\gamma]F_{5/3} \right. \\
 & \left. + \frac{1}{2}[t_5(2x_5+1)\rho^\gamma - t_4(2x_4+1)\rho^\beta]F_{8/3}\right\} \quad (\text{A1})
 \end{aligned}$$

where m is the nucleon mass, k_F is the Fermi momentum of symmetric nuclear matter, i.e.,

$$k_F = \left(\frac{3\pi^2\rho}{2}\right)^{1/3}, \quad (\text{A2})$$

and $F_x(\delta)$ is expressed as

$$F_x(\delta) = \frac{1}{2}[(1+\delta)^x + (1-\delta)^x]. \quad (\text{A3})$$

By setting $\delta = 0$ in Eq. (A1), one can obtain the EOS of symmetric nuclear matter as [22]

$$\begin{aligned}
 E_0(\rho) = & \frac{3\hbar^2}{10m}k_F^2 + \frac{3}{8}t_0\rho + \frac{1}{16}t_3\rho^{\alpha+1} \\
 & + \frac{3}{80}[3t_1 + t_2(4x_2+5)]\rho k_F^2 \\
 & + \frac{3}{80}[3t_4\rho^\beta + t_5(4x_5+5)\rho^\gamma]\rho k_F^2. \quad (\text{A4})
 \end{aligned}$$

The incompressibility K_0 and skewness parameter J_0 of symmetric nuclear matter can then be easily derived with

the following definitions

$$K_0 \equiv 9\rho_0^2 \left. \frac{d^2 E_0(\rho)}{d\rho^2} \right|_{\rho=\rho_0}, \quad (\text{A5})$$

$$J_0 \equiv 27\rho_0^3 \left. \frac{d^3 E_0(\rho)}{d\rho^3} \right|_{\rho=\rho_0}. \quad (\text{A6})$$

The symmetry energy is given by [22]

$$\begin{aligned} E_{\text{sym}}(\rho) &\equiv \frac{1}{2} \left. \frac{\partial^2 E(\rho, \delta)}{\partial \delta^2} \right|_{\delta=0} \\ &= \frac{\hbar^2}{6m} k_F^2 - \frac{1}{8} t_0 (2x_0 + 1) \rho \\ &\quad - \frac{1}{48} t_3 (2x_3 + 1) \rho^{\alpha+1} \\ &\quad - \frac{1}{24} [3t_1 x_1 - t_2 (4 + 5x_2)] \rho k_F^2 \\ &\quad - \frac{1}{24} [3t_4 x_4 \rho^\beta - t_5 (4 + 5x_5) \rho^\gamma] \rho k_F^2, \quad (\text{A7}) \end{aligned}$$

and the density slope of the symmetry energy at a reference density ρ_r can be obtained by the following definition

$$L(\rho_r) \equiv 3\rho_r \left. \frac{dE_{\text{sym}}(\rho)}{d\rho} \right|_{\rho=\rho_r}. \quad (\text{A8})$$

In the extended SHF model, the isoscalar effective mass $m_{s,0}^*$, namely, the effective mass of nucleon in symmetric nuclear matter at saturation density is evaluated by the following relation [22]

$$\begin{aligned} \frac{\hbar^2}{2m_{s,0}^*} &= \frac{\hbar^2}{2m} + \frac{3}{16} t_1 \rho_0 + \frac{1}{16} t_2 (4x_2 + 5) \rho_0 \\ &\quad + \frac{3}{16} t_4 \rho_0^{\beta+1} + \frac{1}{16} t_5 (4x_5 + 5) \rho_0^{\gamma+1}. \quad (\text{A9}) \end{aligned}$$

The value of the isovector effective mass $m_{v,0}^*$, namely, the effective mass of neutron (proton) in pure neutron (proton) matter at saturation density is given by [22]

$$\begin{aligned} \frac{\hbar^2}{2m_{v,0}^*} &= \frac{\hbar^2}{2m} + \frac{1}{8} t_1 (x_1 + 2) \rho_0 + \frac{1}{8} t_2 (x_2 + 2) \rho_0 \\ &\quad + \frac{1}{8} t_4 (x_4 + 2) \rho_0^{\beta+1} + \frac{1}{8} t_5 (x_5 + 2) \rho_0^{\gamma+1} \quad (\text{A10}) \end{aligned}$$

For the finite-range term \mathcal{H}_{fin} in Eq. (3), the gradient coefficient G_S , the symmetry gradient coefficient G_V and the cross gradient coefficient G_{SV} can be obtained as

$$\begin{aligned} G_S &= \frac{9}{32} t_1 - \frac{1}{32} t_2 (4x_2 + 5) \\ &\quad + \frac{3}{32} t_4 (2\beta + 3) \rho_0^\beta - \frac{1}{32} t_5 (4x_5 + 5) \rho_0^\gamma, \quad (\text{A11}) \end{aligned}$$

$$\begin{aligned} G_V &= \frac{3}{32} t_1 (2x_1 + 1) + \frac{1}{32} t_2 (2x_2 + 1) \\ &\quad + \frac{3}{32} t_4 (2x_4 + 1) \rho_0^\beta + \frac{1}{32} t_5 (2x_5 + 1) \rho_0^\gamma, \quad (\text{A12}) \end{aligned}$$

$$G_{SV} = \frac{\beta}{16} t_4 (1 + 2x_4) \rho_0^\beta. \quad (\text{A13})$$

Appendix B: Relationship between the Skyrme parameters and the macroscopic quantities in the extended SHF model

We reexpress the EOS of symmetric nuclear matter (Eq. (A4)) as

$$\begin{aligned} E_0(\rho) &= E_{\text{kin}}^0 \left(\frac{\rho}{\rho_0}\right)^{2/3} + s_0 \frac{\rho}{\rho_0} + (s_1 + s_2) \left(\frac{\rho}{\rho_0}\right)^{5/3} \\ &\quad + s_3 \left(\frac{\rho}{\rho_0}\right)^{\alpha+1} + s_4 \left(\frac{\rho}{\rho_0}\right)^{\beta+5/3} + s_5 \left(\frac{\rho}{\rho_0}\right)^{\gamma+5/3} \quad (\text{B1}) \end{aligned}$$

where we have

$$E_{\text{kin}}^0 = \frac{3\hbar^2}{10m} k_{F,0}^2, \quad (\text{B2})$$

with $k_{F,0} = (3\pi^2 \rho_0 / 2)^{1/3}$ and the coefficients $s_0 \sim s_5$ are defined as

$$\begin{aligned} s_0 &= \frac{3}{8} t_0 \rho_0, & s_3 &= \frac{1}{16} t_3 \rho_0^{\alpha+1}, \\ s_1 &= \frac{9}{80} t_1 \rho_0 k_{F,0}^2, & s_4 &= \frac{9}{80} t_4 \rho_0^{\beta+1} k_{F,0}^2, \\ s_2 &= \frac{3}{80} t_2 (5 + 4x_2) \rho_0 k_{F,0}^2, & s_5 &= \frac{3}{80} t_5 (5 + 4x_5) \rho_0^{\gamma+1} k_{F,0}^2. \end{aligned}$$

Similarly, the symmetry energy (Eq. (A7)) can be rewritten as

$$\begin{aligned} E_{\text{sym}}(\rho) &= E_{\text{kin}}^{\text{sym}} \left(\frac{\rho}{\rho_0}\right)^{2/3} + \omega_0 \frac{\rho}{\rho_0} + (\omega_1 + \omega_2) \left(\frac{\rho}{\rho_0}\right)^{5/3} \\ &\quad + \omega_3 \left(\frac{\rho}{\rho_0}\right)^{\alpha+1} + \omega_4 \left(\frac{\rho}{\rho_0}\right)^{\beta+5/3} + \omega_5 \left(\frac{\rho}{\rho_0}\right)^{\gamma+5/3} \quad (\text{B3}) \end{aligned}$$

where we have

$$E_{\text{kin}}^{\text{sym}} = \frac{\hbar^2}{6m} k_{F,0}^2, \quad (\text{B4})$$

and the coefficients $\omega_0 \sim \omega_5$ are defined as

$$\begin{aligned} \omega_0 &= -\frac{1}{8} t_0 (2x_0 + 1) \rho_0, & \omega_3 &= \frac{1}{48} t_3 (2x_3 + 1) \rho_0^{\alpha+1}, \\ \omega_1 &= -\frac{1}{8} t_1 x_1 \rho_0 k_{F,0}^2, & \omega_4 &= -\frac{1}{8} t_4 x_4 \rho_0^{\beta+1} k_{F,0}^2, \\ \omega_2 &= \frac{1}{24} t_2 (4 + 5x_2) \rho_0 k_{F,0}^2, & \omega_5 &= \frac{1}{24} t_5 (4 + 5x_5) \rho_0^{\gamma+1} k_{F,0}^2. \end{aligned}$$

In the extended SHF model with fixed β and γ , the thirteen coefficients $s_0 \sim s_5$, $\omega_0 \sim \omega_5$ and α can be explicitly expressed in terms of thirteen macroscopic quantities ρ_0 , $E_0(\rho_0)$, K_0 , J_0 , $E_{\text{sym}}(\rho_r)$, $L(\rho_r)$, $K_{\text{sym}}(\rho_r)$, G_S , G_V , G_{SV} , G'_0 , $m_{s,0}^*$ and $m_{v,0}^*$. Before showing the explicit expressions, we define

$$\xi_1 = E_{\text{kin}}^0 \frac{m - m_{s,0}^*}{m_{s,0}^*}, \quad \xi_2 = \frac{20}{9} \xi_1 - \frac{\hbar^2}{2m} \frac{m - m_{v,0}^*}{m_{v,0}^*} k_{F,0}^2,$$

$$A'_0 = \frac{27\hbar^2 \pi^2 G'_0 \rho_0}{4m_{s,0}^* k_{F,0}}, \quad A_S = \frac{6}{5} G_S \rho_0 k_{F,0}^2,$$

$$A_V = 18 G_V \rho_0 k_{F,0}^2, \quad A_{SV} = \frac{1}{\beta} G_{SV} \rho_0 k_{F,0}^2.$$

The $s_0 \sim s_5$, $\omega_0 \sim \omega_5$ and α can then be expressed as

$$\begin{aligned}
s_4 &= \frac{1}{2\beta} (A_S + 4Y_1 - 3\xi_1), \\
s_1 &= \xi_1 - Y_1 - s_4, \\
\alpha &= \frac{-Y_b + \sqrt{Y_b^2 - 4Y_a \cdot Y_c}}{2Y_a}, \\
s_3 &= \frac{27Y_a}{\alpha(3\alpha - 3\gamma - 4)}, \\
s_5 &= [K_0 + 2E_{\text{kin}}^0 - 10\xi_1 - (3\alpha + 3)(E_{\text{kin}} - 3E_0 - 2\xi_1) \\
&\quad - 3\beta(3\beta - 3\alpha + 4)s_4] / [3\gamma(3\gamma - 3\alpha + 4)], \\
s_0 &= E_0 - E_{\text{kin}}^0 - \xi_1 - s_3, \\
s_2 &= Y_1 - s_5, \\
\omega_4 &= \frac{5}{9}s_4 - A_{SV}, \\
\omega_1 &= -\omega_4 - \frac{A'_0}{54} - \frac{A_V}{27} - \frac{E_0}{6} + \frac{E_{\text{kin}}^0}{6} + \frac{4}{9}\xi_1, \\
\omega_3 &= \left\{ Y_2 [(3\gamma + 2)(3\gamma + 5)\eta^{\gamma+5/3} - 10\eta^{5/3}] \right. \\
&\quad \left. - Y_3 [(3\gamma + 2)\eta^{\gamma+5/3} - 2\eta^{5/3}] \right\} \\
&\quad / \left\{ 3\alpha\eta^{\alpha+1} [(3\gamma + 2)(3\gamma - 3\alpha + 2)\eta^{\gamma+5/3} \right. \\
&\quad \left. + (6\alpha - 4)\eta^{5/3}] \right\}, \\
\omega_5 &= [Y_3 - Y_2(3\alpha + 3)] \\
&\quad / \left[(3\gamma + 2)(3\gamma - 3\alpha + 2)\eta^{\gamma+5/3} + 2(3\alpha - 2)\eta^{5/3} \right], \\
\omega_2 &= -\frac{A'_0}{18} - \frac{E_0}{2} + \frac{E_{\text{kin}}^0}{2} - \frac{\xi_1}{3} + \frac{20}{9}Y_1 - \omega_5, \\
\omega_0 &= \eta^{-1}E_{\text{sym}}(\rho_r) - \eta^{-1/3}E_{\text{kin}}^{\text{sym}} - \eta^\alpha\omega_3 \\
&\quad - \eta^{2/3}(\omega_1 + \omega_2) - \eta^{\beta+2/3}\omega_4 - \eta^{\gamma+2/3}\omega_5,
\end{aligned}$$

with

$$\begin{aligned}
\eta &= \frac{\rho_r}{\rho_0}, \\
Y_1 &= \frac{1}{30}A'_0 + \frac{1}{60}A_V + \frac{3}{10}E_0 - \frac{3}{10}E_{\text{kin}}^0 - \frac{1}{20}\xi_1 + \frac{9}{20}\xi_2, \\
Y_2 &= L(\rho_r) - 3E_{\text{sym}}(\rho_r) + \eta^{2/3}E_{\text{kin}}^{\text{sym}} - 2\eta^{5/3}\xi_2 \\
&\quad + \omega_4[2\eta^{5/3} - (3\beta + 2)\eta^{\beta+5/3}], \\
Y_3 &= K_{\text{sym}}(\rho_r) + 2\eta^{2/3}E_{\text{kin}}^{\text{sym}} - 10\eta^{5/3}\xi_2 + \\
&\quad \omega_4 [10\eta^{5/3} - (3\beta + 2)(3\beta + 5)\eta^{\beta+5/3}], \\
Y_a &= 9 [K_0 + 2E_{\text{kin}}^0 - 10\xi_1 - (3\gamma + 7)(E_{\text{kin}}^0 - 3E_0 - 2\xi_1) \\
&\quad - 9\beta(\beta - \gamma)s_4], \\
Y_b &= 9(3\gamma^2 + 6\gamma + 1)(E_{\text{kin}}^0 - 3E_0 - 2\xi_1 - 3\beta s_4) \\
&\quad - 3 [J_0 - 8E_{\text{kin}}^0 + 10\xi_1 - 9\beta(3\beta^2 + 6\beta + 1)s_4], \\
Y_c &= -Y_a - 3(3\gamma^2 + 6\gamma + 1) \\
&\quad \times [K_0 - E_{\text{kin}}^0 + 9E_0 - 4\xi_1 - 3\beta(3\beta + 4)s_4] \\
&\quad + (3\gamma + 4) [J_0 - 8E_{\text{kin}}^0 + 10\xi_1 - 9\beta(3\beta^2 + 6\beta + 1)s_4].
\end{aligned}$$

Once given the thirteen macroscopic quantities, one can obtain $s_0 \sim s_5$, $\omega_0 \sim \omega_5$ and α by invoking the above expressions, and then the Skyrme parameters can be easily obtained.

-
- | | |
|---|--|
| <p>[1] J.M. Lattimer and M. Prakash, <i>Science</i> 304, 536 (2004); <i>Phys. Rep.</i> 442, 109 (2007).</p> <p>[2] A.W. Steiner, M. Prakash, J.M. Lattimer, and P. J. Ellis, <i>Phys. Rep.</i> 411, 325 (2005).</p> <p>[3] V. Baran, M. Colonna, V. Greco, and M. Di Toro, <i>Phys. Rep.</i> 410, 335 (2005).</p> <p>[4] B.A. Li, L.W. Chen, and C.M. Ko, <i>Phys. Rep.</i> 464, 113 (2008).</p> <p>[5] B. ter Haar and R. Malfliet, <i>Phys. Rep.</i> 149, 207 (1987).</p> <p>[6] I. Bombaci and U. Lombardo, <i>Phys. Rev. C</i> 44, 1892 (1991).</p> <p>[7] W. Zuo, I. Bombaci, and U. Lombardo, <i>Phys. Rev. C</i> 60, 024605 (1999).</p> <p>[8] V.R. Pandharipande and R.B. Wiringa, <i>Rev. Mod. Phys.</i> 51, 821 (1979).</p> <p>[9] A. Akmal, V.R. Pandharipande, and D.G. Ravenhall, <i>Phys. Rev. C</i> 58, 1804 (1998).</p> <p>[10] A. Gezerlis <i>et al.</i>, <i>Phys. Rev. Lett.</i> 111, 032501 (2013).</p> | <p>[11] G. Wlazłowski <i>et al.</i>, <i>Phys. Rev. Lett.</i> 113, 182503 (2014).</p> <p>[12] A. Roggero, A. Mukherjee, and F. Pederiva, <i>Phys. Rev. Lett.</i> 112, 221103 (2014).</p> <p>[13] K. Hebeler, J.M. Lattimer, C.J. Pethick, and A. Schwenk, <i>Phys. Rev. Lett.</i> 105, 161102 (2010).</p> <p>[14] I. Tews, T. Krüger, K. Hebeler, and A. Schwenk, <i>Phys. Rev. Lett.</i> 110, 032504 (2013).</p> <p>[15] M. Bender, P.-H. Heenen, and P.-G. Reinhard, <i>Rev. Mod. Phys.</i> 75, 121 (2003).</p> <p>[16] T. H. R. Skyrme, <i>Phil. Mag.</i> 1, 1043 (1956).</p> <p>[17] D. Vautherin and D. M. Brink, <i>Phys. Rev. C</i> 5, 626 (1972).</p> <p>[18] E. Chabanat, P. Bonche, P. Haensel, J. Meyer, and R. Schaeffer, <i>Nucl. Phys.</i> A627, 710 (1997).</p> <p>[19] E. Chabanat, P. Bonche, P. Haensel, J. Meyer, and R. Schaeffer, <i>Nucl. Phys.</i> A635, 231 (1998).</p> <p>[20] L.G. Cao, U. Lombardo, C.W. Shen, and N. Van Giai,</p> |
|---|--|

- Phys. Rev. C **73**, 014313 (2006).
- [21] J.R. Stone and P.-G. Reinhard, Prog. Part. Nucl. Phys. **58**, 587 (2007).
- [22] N. Chamel, S. Goriely, and J.M. Pearson, Phys. Rev. C **80**, 065804 (2009).
- [23] S. Goriely, N. Chamel, and J.M. Pearson, Phys. Rev. C **82**, 035804 (2010).
- [24] M. Dutra *et al.*, Phys. Rev. C **85**, 035201 (2012).
- [25] D. Gambacurta *et al.*, Phys. Rev. C **84**, 024301 (2011).
- [26] J. Erler *et al.*, Phys. Rev. C **87**, 044320 (2013).
- [27] S. Goriely, N. Chamel, and J.M. Pearson, Phys. Rev. C **88**, 024308 (2013).
- [28] M. Baldo, L.M. Robledo, P. Schuck, and X. Viñas, Phys. Rev. C **87**, 064305 (2013).
- [29] W.C. Chen and J. Piekarewicz, Phys. Rev. C **90**, 044305 (2014).
- [30] S. Goriely, Nucl. Phys. **A933**, 68 (2015).
- [31] P.B. Demorest, T. Pennucci, S.M. Ransom, M.S.E. Roberts, and J.W.T. Hessels, Nature (London) **467**, 1081 (2010).
- [32] J. Antoniadis *et al.*, Science **340**, 448 (2013).
- [33] D.H. Youngblood, H.L. Clark, and Y.W. Lui, Phys. Rev. Lett. **82**, 691 (1999).
- [34] T. Li *et al.*, Phys. Rev. Lett. **99**, 162503 (2007).
- [35] D. Patel *et al.*, Phys. Lett. **B726**, 178 (2013).
- [36] P. Danielewicz, R. Lacey, and W.G. Lynch, Science **298**, 1592 (2002).
- [37] C. Fuchs, Prog. Part. Nucl. Phys. **56**, 1 (2006).
- [38] J. Aichelin and C. M. Ko, Phys. Rev. Lett. **55**, 2661 (1985).
- [39] D.W. Wen, B.A. Li, and L.W. Chen, Phys. Rev. Lett. **103**, 211102 (2009).
- [40] M. I. Krivoruchenko, F. Simkovic, and A. Faessler, Phys. Rev. D **79**, 125023 (2009).
- [41] D.R. Zhang, P.L. Yin, W. Wang, Q.C. Wang, and W.Z. Jiang, Phys. Rev. D **83**, 035801 (2011).
- [42] H. Zheng and L.W. Chen, Phys. Rev. D **85**, 043013 (2012).
- [43] C.J. Horowitz and J. Piekarewicz, Phys. Rev. Lett. **86**, 5647 (2001).
- [44] R.J. Furnstahl, Nucl. Phys. **A706**, 85 (2002).
- [45] N. Wang, L. Ou, and M. Liu, Phys. Rev. C **87**, 034327 (2013).
- [46] P. Danielewicz and J. Lee, Nucl. Phys. **A922**, 1 (2014).
- [47] Z. Zhang and L.W. Chen, Phys. Lett. **B726**, 234 (2013).
- [48] B.A. Brown, Phys. Rev. Lett. **111**, 232502 (2013).
- [49] Z. Zhang and L.W. Chen, Phys. Rev. C **92**, 031301(R) (2015).
- [50] M.B. Tsang *et al.*, Phys. Rev. Lett. **102**, 122701 (2009).
- [51] N. Chamel and S. Goriely, Phys. Rev. C **84**, 045804 (2010).
- [52] J. Margueron, J. Navarro, and N. Van Giai, Phys. Rev. C **66**, 014303 (2002).
- [53] I. Vidaña, A. Polls, and A. Ramos, Phys. Rev. C **65**, 035804 (2002); I. Vidaña and I. Bombaci, Phys. Rev. C **66**, 045801 (2002).
- [54] F. Sammarruca and P.G. Krastev, Phys. Rev. C **75**, 034315 (2007).
- [55] S. Fantoni, A. Sarsa, and K.E. Schmidt, Phys. Rev. Lett. **87**, 181101 (2001).
- [56] F. Sammarruca, R. Machleidt, and N. Kaiser, Phys. Rev. C **92**, 054327 (2015).
- [57] G.H. Bordbar and M. Bigdeli, Phys. Rev. C **77**, 015805 (2008).
- [58] J. Margueron and H. Sagawa, J. Phys. G **36**, 125102 (2009).
- [59] M. Bender, J. Dobaczewski, J. Engel, and W. Nazarewicz, Phys. Rev. C **65**, 054322 (2002).
- [60] P. D. Stevenson, P. M. Goddard, J. R. Stone, and M. Dutra, AIP Conf. Proc. **1529**, 262 (2013).
- [61] S. Krewald, V. Klemt, J. Speth, and A. Faessler, Nucl. Phys. **A281**, 166 (1977).
- [62] L.X. Ge, Y. Z. Zhuo, and W. Norenberg, Nucl. Phys. **A459**, 77 (1986).
- [63] Y.Z. Zhuo, Y.L. Han, and X.Z. Wu, Prog. Theor. Phys. **79**, 110 (1988).
- [64] B.K. Agrawal, S. Shlomo, and V.K. Au, Phys. Rev. C **72**, 014310 (2005).
- [65] M. Waroquier, J. Sau, K. Heyde, P. Van Isacker, and H. Vincx, Phys. Rev. C **19**, 1983 (1979).
- [66] P. Ring and P. Schuck, *The Nuclear Many-Body Problems*, Springer-Verlag, New York, 1980.
- [67] L.W. Chen, B.J. Cai, C.M. Ko, B.A. Li, C. Shen, and J. Xu, Phys. Rev. C **80**, 014322 (2009).
- [68] L.W. Chen, C.M. Ko, B.A. Li, and J. Xu, Phys. Rev. C **82**, 024321 (2010).
- [69] L.W. Chen, Sci. China: Phys. Mech. Astron. **54**, s124 (2011).
- [70] B.J. Cai and L.W. Chen, arXiv:1402.4242.
- [71] F. Osterfeld, Rev. Mod. Phys. **64**, 491 (1992).
- [72] M. Baldo, U. Lombardo, E. E. Saperstein, and M. V. Zverev, Phys. Lett. **B421**, 8 (1998).
- [73] W. Zuo, C.W. Shen, and U. Lombardo, Phys. Rev. C **67**, 037301 (2003).
- [74] C.W. Shen, U. Lombardo, N. Van Giai, and W. Zuo, Phys. Rev. C **68**, 055802 (2003).
- [75] T. Wakasa, M. Ichimura, and H. Sakai, Phys. Rev. C **72**, 067303 (2005).
- [76] I. N. Borzov, Nucl. Phys. **A777**, 645 (2006).
- [77] A. Bohr and B. Mottelson, *Nuclear Structure* (Benjamin, London, 1975), Vol. II.
- [78] O. Bohigas, A. M. Lane, and J. Martorell, Phys. Rep. **51**, 267 (1979).
- [79] T. Sil, S. Shlomo, B.K. Agrawal, and P.-G. Reinhard, Phys. Rev. C **73**, 034316 (2006).
- [80] M. Wang *et al.*, Chin. Phys. C **36**, 1287 (2012).
- [81] I. Angeli, At. Data Nucl. Data. Tables **87**, 185 (2004).
- [82] F. Le Blanc *et al.*, Phys. Rev. C **72**, 034305 (2005).
- [83] Z. Zhang and L.W. Chen, Phys. Rev. C **90**, 064317 (2014).
- [84] Z. Zhang and L.W. Chen, Phys. Rev. C **93**, 034335 (2016).
- [85] C. Xu, B.A. Li, and L.W. Chen, Phys. Rev. C **82**, 054607 (2010).
- [86] X.H. Li, W.J. Guo, B.A. Li, L.W. Chen, F.J. Fattoyev, and W.G. Newton, Phys. Lett. **B743**, 408 (2015).
- [87] Z.H. Li and H.-J. Schulze, Phys. Rev. C **78**, 028801 (2008).
- [88] <http://www-astro.ulb.ac.be/bruslib/nucdata/>
- [89] R. Klüpfel, P.-G. Reinhard, T.J. Bürvenich, and J.A. Maruhn, Phys. Rev. C **79**, 034310 (2009).
- [90] B. A. Brown, Phys. Rev. Lett. **85**, 5296 (2000).
- [91] S. Typel and B. A. Brown, Phys. Rev. C **64**, 027302 (2001).
- [92] L.W. Chen, C. M. Ko, and B.-A. Li, Phys. Rev. C **72**, 064309 (2005).
- [93] X. Roca-Maza *et al.*, Phys. Rev. C **88**, 024316 (2013).
- [94] C.M. Tarbert *et al.*, Phys. Reiv. Lett. **112**, 242502

- (2014).
- [95] S. Abrahamyan *et al.*, Phys. Rev. Lett **108**, 112502 (2012).
- [96] M. Bender, W. Nazarewicz, and P.-G. Reinhard, Phys. Lett. **B515**, 42 (2001).
- [97] B.M. Tsang *et al.*, Phys. Rev. C **86**, 015803 (2012).
- [98] J.M. Lattimer, Ann. Rev. Nucl. Part. Sci. **62**, 485 (2012).
- [99] L.W. Chen, in Nuclear Structure in China (2012), *Proceedings of the 14th National Conference on Nuclear Structure in China (NSC2012), Hu-Zhou, Zhejiang, China, 2012*, edited by J.Meng, C.-W. Shen, E.-G. Zhao, and S.-H. Zhou (World Scientific, Singapore, 2012), pp. 43 - 54 [arXiv:1212.0284].
- [100] B.A. Li *et al.*, J. Phys.: Conf. Series **413**, 012021 (2013) [arXiv:1212.1178].
- [101] J.P. Blaizot, Phys. Rep. **64**, 171 (1980).
- [102] T. Li *et al.*, Phys. Rev. C **81**, 034309 (2010).
- [103] D. Patel *et al.*, Phys. Lett. **B718**, 447 (2012).
- [104] J.R. Stone, N.J. Stone, and S.A. Moszkowski, Phys. Rev. C **89**, 044316 (2014).
- [105] J.M. Pearson, N. Chamel, and S. Goriely, Phys. Rev. C **82**, 037301 (2010).
- [106] L.W. Chen, C.M. Ko, and B.A. Li, Phys. Rev. Lett. **94**, 032701 (2005).
- [107] L.W. Chen, EPJ Web of Conf. **88**, 00017 (2015) [arXiv:1506.09057].
- [108] E. Suraud, C. Gregoire, and B. Tamain, Prog. Part. Nucl. Phys. **23**, 357 (1989).
- [109] F.S. Zhang and E. Suraud, Phys. Rev. C **51**, 3201 (1995).
- [110] R.C. Tolman, Phys. Rev. **55**, 364 (1939).
- [111] J.R. Oppenheimer and G.M. Volkoff, Phys. Rev. **55**, 374 (1939).
- [112] G. Baym, C.J. Pethick, and P. Sutherland, Astrophys. J. **170**, 299 (1971).
- [113] J. Carrier, C.J. Horowitz, and J. Piekarewicz, Astrophys. J. **593**, 463 (2003).
- [114] J. Xu, L. W. Chen, B. A. Li, and H. R. Ma, Phys. Rev. C **79**, 035802 (2009); Astrophys. J. **697**, 1549 (2009).
- [115] A.W. Steiner, J.M. Lattimer, and E.F. Brown, Astrophys. J. **722**, 33 (2010).
- [116] V. Suleimanov, J. Poutanen, M. Revnivtsev, and K. Werner, Astrophys. J. **742**, 122 (2011).
- [117] S. Guillot, M. Servillat, N. A. Webb, and R. E. Rutledge, Astrophys. J. **772**, 7 (2013).
- [118] J.M. Lattimer and A.W. Steiner, Astrophys. J. **784**, 123 (2014).
- [119] J.M. Lattimer and M. Prakash, Astrophys. J. **550**, 426 (2001).